AN ABSTRACT OF THE THESIS OF

<u>CHARLES RANSFORD BECKER</u> for the <u>DOCTOR OF PHILOSOPHY</u>
(Name)   (Degree)

in <u>CHEMISTRY (PHYSICAL)</u> presented on <u>May 29, 1968</u>
(Major)   (Date)

Title: <u>AN INVESTIGATION OF THE METABORATE MONOMER AND</u>

<u>TRIMER IONS IN ALKALI HALIDE CRYSTALS</u>

Abstract approved: ████████████████████
                                   W. J. Fredericks

The infrared spectra of the metaborate monomer and trimer

ions in NaCl, KCl, and KBr were studied. These spectra contain

bands due to the trimer in solid solution, in a second phase of the ap-

propriate potassium or sodium salt, and perhaps on adjacent lattice

sites. Furthermore, complex equilibria exist between the trimer in

these three forms and the monomer. These equilibria depend upon the

lattice, the boron concentration, and the thermal history of the crys-

tal. The presence of the second phase and its relationship to the in-

frared bands was confirmed with light scattering experiments.

A model for the trimer in solid solution is proposed in which

the planar trimer, $(BO_2^-)_3$, replaces three next nearest neighbor

halide ions that form an equilateral triangle. Moreover, the trimer

is most soluble in KCl consistent with the argument that the solubility

should be greater when the fixed distances between the three negative

charges on the trimer more closely approach the anion-anion distance in the lattice. In contrast, the solubility of the monomer increases as the size of the lattice increases from NaCl to KBr.

A normal coordinate analysis which employes a general valence force field predicts eigenvalues which are in fair agreement with the assigned values of the fundamentals, even though most of the force constants were either borrowed from related compounds or estimated.

Values for the absorption coefficients of the monomer (ω_3) in KCl and KBr, and the trimer (ω_6 and ω_7) in KCl were determined.

An Investigation of the Metaborate Monomer and
Trimer Ions in Alkali Halide Crystals

by

Charles Ransford Becker

A THESIS

submitted to

Oregon State University

in partial fulfillment of
the requirements for the
degree of

Doctor of Philosophy

June 1969

APPROVED:

<div style="text-align: center">████████████████</div>

Professor of Physical Chemistry

in charge of major

<div style="text-align: center">████████████████</div>

Chairman of Department of Chemistry

<div style="text-align: center">████████████████</div>

Dean of Graduate School

Date thesis is presented _May 29, 1968_

Typed by Clover Redfern for   Charles Ransford Becker

To Pamela

ACKNOWLEDGMENTS

TABLE OF CONTENTS

LIST OF TABLES

LIST OF FIGURES

AN INVESTIGATION OF THE METABORATE MONOMER
AND TRIMER IONS IN ALKALI HALIDE CRYSTALS

I. GENERAL INTRODUCTION

An investigation of the structure of a polyatomic ion in solid so-
lution has distinct advantages compared to an investigation of the ion
in a pure crystal of a salt of the ion. Isolation of these ions in a
crystal of a different compound reduces interactions between the ions
in solution and between fundamental vibrations of the ion and lattice
modes of the crystal. This results in bandwidths which are often
comparable to those of a gas. If the symmetry of the site where the
ion is located is lower than the symmetry of the ion, then degenera-
cies may be removed and inactive modes may become weakly active,
giving additional information about the structure. However, it is dif-
ficult to study the structure of an ion in solid solution by independent
means such as Raman scattering, NMR, X-ray diffraction, and others
because the concentration of the ion is usually near or below the sen-
sitivity limits of these methods.

The crystal structures of potassium and sodium metaborate
have been determined by Zachariasen (45) and Fang (14, 15) respec-
tively to be rhombohedral with space group D_{3d}^6 or $R\bar{3}c$. The meta-
borate ion was found to exist as a planar trimer with D_{3h} symmetry
in which three BO_3 groups share corner oxygen atoms and thus form

a six membered ring as shown in Figure 9. Goubeau and Keller (25)

recorded and assigned the Raman spectra of B_3O_3 $(OCH_3)_3$,

$B_3O_3[N(CH_3)_2]_3$, $B_3O_3(CH_3)_3$, and $B_3O_3Cl_3$ whose hexagonal ring

structures are similar to those of potassium and sodium metaborate;

see the summary of assignments in Table 1. Later Goubeau and

Hummel (24) recorded and assigned the infrared spectra of $B_3O_3(CH_3)_3$,

$B_3O_3(OH)_3$, $B_3O_3(OD)_3$, and $(B_3O_6)Na_3$ in either KBr pellets or nujol

mulls. They concluded that the infrared spectra of orthorhombic

metaboric acid and its sodium salt are very similar to that of tri-

methylboroxine, just as is the case for the Raman spectra of the es-

ters of orthorhombic metaboric acid and trimethylboroxine. Parsons

(33) re-examined the spectra of orthorhombic metaboric acid in nujol

mulls and made a new assignment for the metaborate trimer ion,

$(BO_2^-)_3$. The infrared spectra limited to the rock salt region and

assignments of trifluoroboroxine published by Fisher, Lehmann, and

Shapiro (17) are in good agreement with those of Parsons. Later Lat-

imer and Devlin (29) extended this work to 250 cm^{-1} on thin films of

trifluoroboroxine, and their data and assignments are in qualitative

agreement with Fisher et al. . They also studied and made an as-

signment of the infrared spectra of trichloroboroxine. Büchler and

Marram (5) obtained the spectrum of sodium metaborate which was

condensed from the vapor, and most of the experimental lines agree

with those of Goubeau and Hummel. The infrared spectra of the

Table 1. Previous assignments for metaborate trimer ion, $(BO_2^-)_3$, and related compounds.

(a) Goubeau and Keller (25)
(b) Goubeau and Hummel (24)
(c) Parsons (33)
(d) Fisher, Lehmann and Shapiro (17)
(e) Latimer and Devlin (29)
(f) Büchler and Marram (5)
(g) Hisatsune and Suarez, in KBr pellet (28)

[1] Obscured by stong OH⁻ absorbance

[2] Activated in solid state infrared

[3] Estimated

s = strong
m = medium
w = weak
v = very
b = broad
sh = shoulder

		Raman(a) $B_3O_3Cl_3$	Raman (a) $B_3O_3[N(CH_3)_2]_3$	Raman (b) $B_3O_3(CH_3)_3$	IR (b) $B_3O_3(CH_3)_3$	Raman (a) $B_3O_3(OCH_3)_3$	IR (b) $B_3O_3(OH)_3$	IR (b) $B_3O_3(OD)_3$	IR (c) $B_3O_3(OH)_3$	IR (c) $^{10}B_3O_3(OH)_3$	IR (c) $B_3O_3(OD)_3$
A_1'	ω_1	1037	1147	1155		1286			1239	1267	1226
	ω_2	807	804	807		804			1/	1/	805
	ω_3	333	537	539		556			595	600	577
A_2'	ω_4								1473	1523	1441
	ω_5								478	482	474
E'	ω_6		1355		1384 vs		1375vs, vb	1350vs, vb	1397	1451	1407
	ω_7				1226 s		1150 m	1160w, vb	1342 1360	1385	1358
	ω_8				783 m		735 s, b	718 s, b	939	942	930
	ω_9	390	433	451	450 vs	403	456 s		462	463	456
	ω_{10}	150		232		257	280 m				
A_2''	ω_{11}				570 s		591 m		745	761	727 739
	ω_{12}				459 m		476 m				
E''	ω_{13}			597		350			650	675	639
	ω_{14}			170		156					

Table 1. Continued.

		IR(d) $^{11}B_3O_3(CH_3)_3$	IR(d) $^{10}B_3O_3(CH_3)_3$	IR(d) $^{11}B_3O_3F_3$	IR(d) $^{10}B_3O_3F_3$	IR(e) $^{11}B_3O_3F_3$	IR(e) $^{10}B_3O_3F_3$	IR(e) $^{11}B_3O_3Cl_3$	IR(e) $^{10}B_3O_3Cl_3$	IR(b) $B_3O_6Na_3$	IR(f) $B_3O_6Na_3$	IR(g) $(^{11}BO_2^-)_3$	IR(g) $(^{10}BO_2^-)_3$
A_1'	ω_1											1138	1210
	ω_2					826 [2/]	838 [2/]		815 [2/]			823	837
	ω_3											616	633
A_2'	ω_4											690	708
	ω_5											455	460
E'	ω_6	1384	1430	1450 s, b	1477	1436	1468	1345	1385	1425vs, b 1450vs, b	1460s, b	1400	1460
	ω_7	1227	1260	1381 s, b	1431	1373	1403	1183	1220	1227s, b 1255s, b	1235s, b	1222	1265
	ω_8	918	942	966 m	968	964	966	760	765	702 w 720 w	700 w 720 w	950	957
	ω_9					462	465	390	392			473	478
	ω_{10}					316	319					200 [3/]	205 [3/]
A_2''	ω_{11}	784	786	714 s, b	733	711	731	664	686			728	754
	ω_{12}											387	388
E''	ω_{13}											717	717
	ω_{14}											280 [3/]	280 [3/]

metaborate trimer ion in pressed disks of alkali halides were observed by Hisatsune and Suarez (28). The trimer ions were prepared directly in the alkali halide matrices by the oxidation of BH_4^- with either trapped atmospheric oxygen, $KClO_3$, or $KClO_4$. They concluded that the trimer ion was in solid solution; however, the published fundamentals reproduced in Table 2 do not show a lattice effect in either sodium halides or potassium halides suggesting the trimer ion was in a second phase of $Na_3(BO_2)_3$ or $K_3(BO_2)_3$ respectively.

Table 2. Matrix effects on some $(BO_2^-)_3$ fundamentals at 25° C published by Hisatsune and Suarez.

	NaCl	NaBr	NaI	KCl	KBr	KI
ω_6	1466	1465	1462	1440	1440	1439
	1436	1439	1434	1405	1405	1405
ω_7	1264	1264	1260	1250	1249	1250
	1241	1240	1239	1225	1225	1228
ω_{11}	724	721	722	735	734	734
	708	706	708	717	717	717

Single crystals of alkali halides containing metaborate trimer ions in solid solution were grown allowing the present infrared investigation to be conducted. A normal coordinate analysis of the metaborate trimer ion was also carried out using a general valence force field.

II. EXPERIMENTAL TECHNIQUES AND EQUIPMENT

Sample Preparations

Materials

Reagent grade KCl and NaCl were purified by an ion exchange process originally developed by Fredericks, Rosztoczy, and Hatchett (18) for KCl. This was modified later by Fredericks, Schuerman, and Lewis (19) for both KCl and NaCl. Infrared quality KBr and CsI obtained from the Harshaw Company were used without further purification.

The doping materials consisted of $LaBO_3$, KBO_2, $NaBO_2$, H_3BO_3, glassy B_2O_3, and crystalline B_2O_3. $LaBO_3$ was prepared using a modification of the method of Goldschmidt and Hauptmann (23). A solution of H_3BO_3 and chemically pure $LaCl_3$ was evaporated to dryness, and the product was heated to red heat for five or ten minutes. An infrared spectrum of a nujol mull of the final product is in good agreement with the spectra of $LaBO_3$ published by Steele and Decius (39). Both KBO_2 and $NaBO_2$ were produced by evaporating to dryness a solution of H_3BO_3 and the appropriate reagent grade alkali metal hydroxide as suggested by Cole, Scholes, and Ambery (6). In order to prepare crystalline B_2O_3, reagent grade boric acid was held at 150° C for three weeks in a platinum crucible; the temperature was

subsequently increased to 200° C at a rate of 10° C per day, and finally it was held at 500° C for one day. Glassy B_2O_3 was prepared by merely heating reagent grade boric acid until molten in a platinum crucible.

Reagent grade boric acid which consequently contains boron isotopes in natural abundance was employed, while the isotopically enriched forms of boron were obtained from the Oak Ridge National Laboratory. The enriched ^{11}B in the form of boric acid was reported to contaion 97.42% of ^{11}B, whereas the enriched ^{10}B was elemental boron and stated to contain 96% of ^{10}B. H_3BO_3 containing enriched ^{10}B was made by the oxidation of elemental ^{10}B with excess concentrated nitric acid. The solution was diluted, activated charcoal was added and then removed by filtration, and finally the solution was evaporated to dryness which resulted in the volatilization of the excess nitric acid.

The preparation of $K_3(BO_2)_3$ crystals was accomplished as described by Zachariasen (45) by fusing K_2CO_3 and H_3BO_3 in a platinum crucible and rapidly cooling the melt. The product was broken open and the small clear crystals were removed. Crystals of $Ca(BO_2)_2$ were prepared in the same manner using CaO after the method of Goubeau and Hummel (24). Standard mull techniques were used in obtaining the spectra of $K_3(BO_2)_3$ and $Ca(BO_2)_2$.

Crystal Growth

The alkali halide crystals were grown by the Stockbarger method in both Vycor and quartz growth tubes. Quartz was occasionally employed because of the isotopic dilution of the enriched boron which occurred when Vycor was used. The Vycor employed in these experiments consisted of 96% silica and 4% boric oxide, alumina, and other impurities; whereas the quartz was relatively pure SiO_2. The quartz tubing was type 204 clear fused quartz obtained from the General Electric Company and was reported to contain an average of 0.5 ppm and a maximum of 0.6 ppm of boron. A tapped Marshall metallurgical testing furnace which is Kanthal wound, is 16 inches long, and has an inside diameter of three inches was used for cyrstal growth. The furnace was shunted and a stainless steel sleeve was placed in the bottom of the furnace to provide a temperature gradient. The furnace was controlled to within ± one degree centigrade with a continuous power regulator consisting of a model 407 Wheelco controller and a 620A silicon controlled rectifier. The growth tubes were dropped through the temperature gradient at a speed of 0.4 cm/hr. with a synchronous motor using a chain drive.

The growth tubes filled with either KCl or NaCl were placed on a vacuum system and evacuated at 150° C. An HCl atmosphere was added and removed two or three times both at 150° C and 400° C to

remove most of the water present. The salt was then melted with an HCl atmosphere in order to remove the remaining H_2O. The HCl was removed and Cl_2 was subsequently added to form covalent chlorides of any heavy metals present which being volatile were then removed by sublimation. Because monovalent ions are more difficult to remove than polyvalent ions by the ion exchange process (19), this step mainly removes monovalent metal ions which form covalent chlorides after being oxidized to higher valence states. Growth tubes containing KBr and CsI were merely evacuated at 150° C and 400° C for 12 hours or more to remove most of the water present. The doping material was then added, and the growth tube was sealed while under a vacuum. The final steps were slightly altered for two KCl crystals. In this case, the doping materials consisting of H_3BO_3 and excess reagent grade KOH were added to the melt. After a short time an HCl atmosphere was added to remove the excess OH^- with the ensuing water being removed by evacuation before the tube was sealed.

After removal from the growth tube the cyrstals were cooled to room temperature by merely allowing them to lose heat to the atmosphere. Although most observations were made on crystals with this thermal history, some measurements were made on crystals which had been quenched rapidly to the boiling point of nitrogen or annealed slowly. Single crystals wrapped in platinum foil were held at some temperature near the melting point, e.g. 605° C for KCl, between 1

and 24 hours and then were placed in a copper container filled with

liquid nitrogen. A precooled copper weight was placed on top of the

cyrstal to prevent bubbles of gaseous nitrogen from insulating the

crystal from the copper. Crystals in an evacuated quartz tube were

annealed by lowering the temperature from a temperature near the

melting point to approximately $250°$ C at the rate of about $12°$ C per

hour.

Measurements

Optical

Beckman IR-7 and IR-11 spectrophotometers (3, 4) were used

in the near IR, 650-4000 cm^{-1}, and the far IR, 33-650 cm^{-1}, respec-

tively; but host absorbance limited range to > 450 cm^{-1} in KCl and to

> 280 cm^{-1} in KBr. Both are double beam instruments and are simi-

lar electronically. The IR-7 utilizes double prism dispersion for pri-

mary separation of the wavelengths and a grating for final dispersion

of the light. A 60 x 75 mm, $60°$, NaCl foreprism and a 64 x 64 mm

replica grating with 75 lines per mm and a 12 μ blaze were used. The

resolution of the IR-7 for the actual scanning conditions was about one

cm^{-1}. The monochromator in the IR-11 is a filter and grating device

which uses a combination of one of four different gratings and one of

eight filters. The resolution of the IR-11 for the actual scanning

conditions was $< 2.5 \text{ cm}^{-1}$.

Most of the infrared spectra were taken while the samples were cooled to near the boiling point of liquid nitrogen. Both a pyrex cold cell and a commercial liquid helium cold cell with alkali halide windows were used. Soft indium spacers ensured good thermal contact between the crystalline sample and the brass sample holder.

A model 450 Perkin-Elmer spectrophotometer (35) was used in the U. V. and far U. V. regions. It is a double beam instrument employing matched detectors. The monochromator consists of two quartz prisms, and the instrument is capable of resolution better than one $\overset{\circ}{\text{A}}$ in the region of interest, 175-250 mμ.

Defect scattering of U. V. and visible light in doped KBr and NaCl, thought to be due to a precipitate or second phase, was observed and photographed by means of an ultramicroscope. The ultramicroscope consists of an optical bench with a variable lens (10-40X) and a variable slit, a zenon lamp, and a Tiyoda research microscope. The photographs, including several of a stage micrometer for calibration purposes, were taken with a single lens, reflex camera made by the Honeywell Pentax Company. Quantitative measurements of the defect scattering were made using a recording polarization spectrometer built by Evett and Isenberg (13). The incident light was vertically polarized, and the vertical and horizontal components of the scattered light were measured separately. Defect scattering should

depolarize the light, whereas scattering from surfaces should not. Therefore, the ratio of the scattered horizontal component to the scattered vertical component EB/EE is a measure of light scattering by defects which depolarizes the light. Information about the size of the defects was not available from this experiment because the wavelength dependence of the scattered bands was caused by the instrument.

Concentration of Boron

The concentration of boron in alkali halide crystals was determined by means of a colorimetric method developed by Hatcher and Wilcox (26). This method uses carminic acid which changes from an absorption at 520 mμ to one at 585 mμ in the presence of boron and its effective range is one to ten μg of boron.

III. EXPERIMENTAL RESULTS AND DISCUSSION

Introduction

The initial infrared spectra were obtained from KCl crystals grown in Vycor growth tubes and doped with OH^-. Because it was quite evident that the OH^- had chemically reacted with the Vycor, the source of the impurity was proposed to be the Vycor tube which contains 4% boric oxide, alumina, and other impurities. The spectra contained intense bands which were attributed to the linear, symmetric metaborate monomer ion (31, 32), indicating that the OH^- had reacted with the boric oxide in the Vycor to produce the metaborate monomer. Furthermore, this suggested that the unknown portion of the spectra was due to some impurity which contained boron. In order to substantiate this, KCl and KBr crystals were doped with boron in the form of $LaBO_3$, KBO_2, glassy B_2O_3, crystalline B_2O_3, and boric acid. Spectra similar to the original spectra were obtained when the doping materials were $LaBO_3$ and KBO_2, and appropriate shifts in the bands for different isotopic ratios of ^{10}B to ^{11}B demonstrated that the impurity does contain boron; see Figure 1. The bands were much more intense when KBO_2 was employed rather than $LaBO_3$, as is expected, because a large amount of electrostatic energy is required to place a trivalent ion such as La^{+3} or BO_3^{-3} on a monovalent lattice site. In addition, some of the fundamentals were observed to

have at least four isotopic components demonstrating that the impurity contains more than one boron atom. When B_2O_3 and boric acid were used, only weak and extremely broad bands were observed except for the very sharp lines of the metaborate monomer. These broad bands may be due to a small amount of polymer or an amorphous second phase. Thus, the impurity was introduced only when the dopant contained some ionic form of boron and oxygen, and therefore we infer that the impurity is ionic. Boric acid exists in the three forms H_3BO_3, HBO_2, and B_2O_3 and being a very weak acid may be considered a neutral molecule. This inference is by no means conclusive, even though the introduction of a charged impurity substitutionally is energetically more favorable. The impurity may occupy an interstitial position; however, the amount of space available at such a position is small. Consequently, this would impose restrictions on the size and shape of the impurity. A neutral molecule which may be coordinated interstitially to four chloride ions is considered in a following section.

The amount of OH^- present was small compared to the amount of KBO_2 added or thought present in crystals doped with OH^-. The concentration of OH^- was determined from an electronic transition at 204 mμ in KCl using an absorption coefficient published by Gie and Klein (22). This band at 204 mμ in KCl and 215 mμ in KBr was shown to be due to OH^- by Fritz, Lüty, and Anger (20) and Rolfe (37)

respectively. In one KCl crystal doped with OH⁻, the concentration of the remaining OH⁻ was 13 ppm, and most of the crystals doped with KBO_2 contained 2-4 ppm or less. This may be compared with the amount of boron present which was found colorimetrically to be approximately 50-200 ppm depending upon the position of the sample in the crystal. If this electronic transition is nearly the same for free OH⁻ isolated in the lattice and OH⁻ as part of a larger ion also isolated in the lattice, as expected, then it is possible to conclude that the impurities present do not contain hydroxide groups. Moreover, when KCl was doped with H_3BO_3 and KOH and subsequently treated with HCl to remove the excess KOH, the same infrared spectra were obtained.

There is evidence from the intensities of the bands that there are three impurities present in addition to the metaborate monomer. These have been designated species A, B, and C. The bands due to A and B are very sharp whereas those due to C are quite broad. Their relative concentrations depend on the host lattice, the concentration of boron, and the thermal history of the crystal. The effect of boron concentration may be conveniently studied in samples taken from different parts of the same crystal, thereby maintaining the same isotopic ratio of boron. This is possible because the solubility of an impurity is usually greater in the liquid phase than in the crystalline phase. Hence the part of the crystal grown last would have a

larger concentration of impurities. A brief discussion of these effects follows, and the appropriate spectra are given in Figures 2, 3, and 4; but a more detailed discussion will be deferred until models for each of these impurities have been considered. The spectra in Figures 1 through 4 correspond to samples near the boiling point of liquid nitrogen except for the portions containing ω_3 of the metaborate monomer, 1900-2100 cm^{-1}, which were observed at room temperature.

Even though the predominant features in spectra of KCl are due to A, the bands which have been assigned to B and C become more intense relative to A as the concentration of impurities increases. The broad bands of C are much weaker than either A or B. In the most concentrated samples available some of the stronger bands of B are comparable to those of A, but in the most dilute samples these same bands are very weak. Conversely, the metaborate monomer ion, BO_2^-, is much more concentrated in the more dilute samples. These observations suggest equilibria exist between at least two and perhaps all four impurities. With the NaCl and KBr matrices the sharp and relatively weaker features of A are superimposed on the strong, broad bands of C. Due to the complexity of the spectra it is difficult to determine whether B is present or not. Later in this chapter, species C is proposed to be a precipitate of the sodium or potassium salt of species A. If this is true, it may be concluded that of these three alkali halides KCl is the optimum host lattice for species A. This is

Figure 1. Spectra of boron containing species in KCl at
various compositions of isotopic boron taken at
$T \simeq 100°$ K. ^{11}B is equal to the fraction of
^{11}B present.
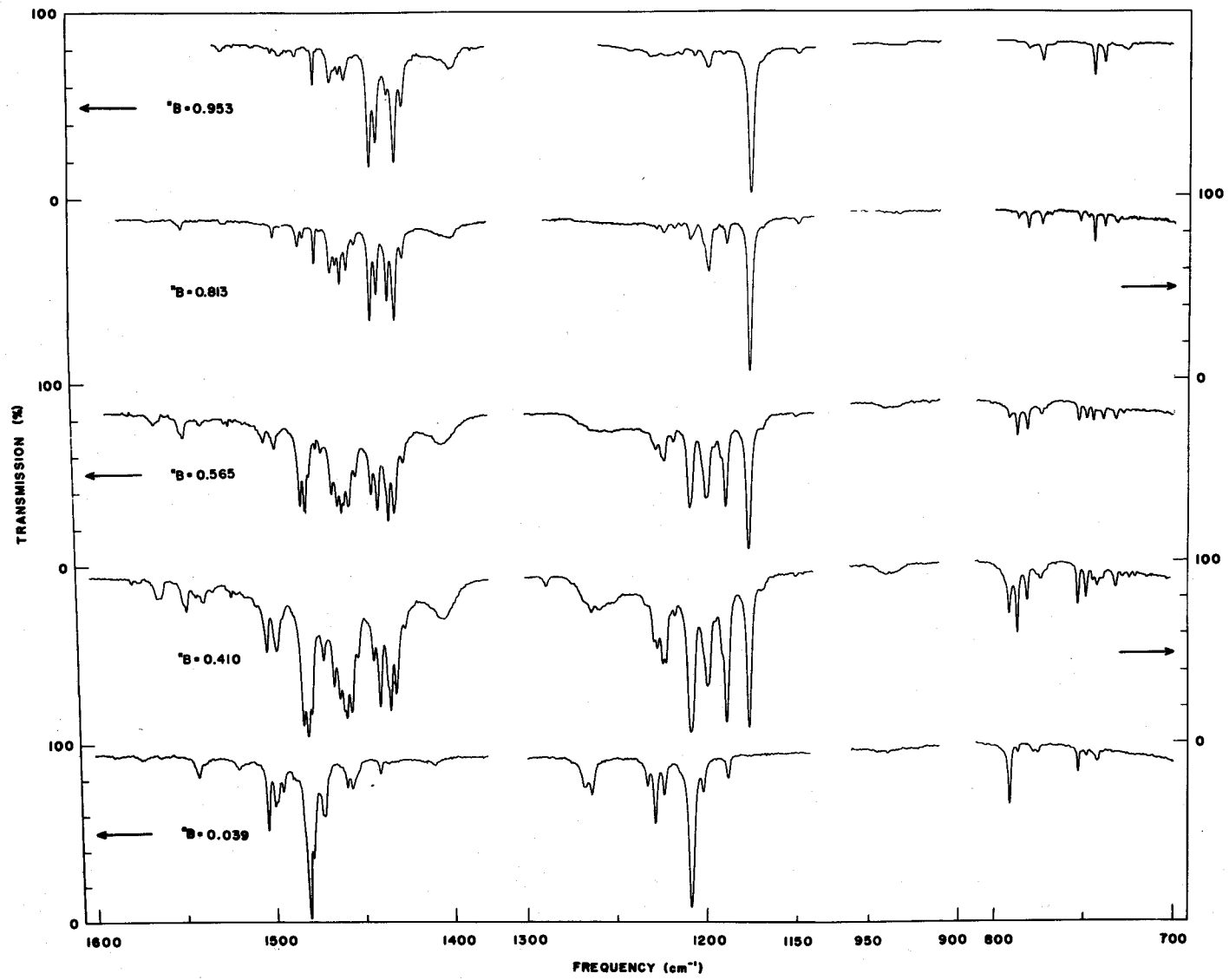
Figure 2. Spectra of boron containing species in NaCl, KCl, and KBr taken at $T \simeq 100°$ K (700-1600 cm^{-1}) and $T \simeq 300°$ K (1930-2080 cm^{-1}) which demonstrate the effect of thermal history upon the equilibria between species.

a. (before quenching), b. (after quenching from 605° C), and c. (after annealing) denote the thermal history of a particular crystal.
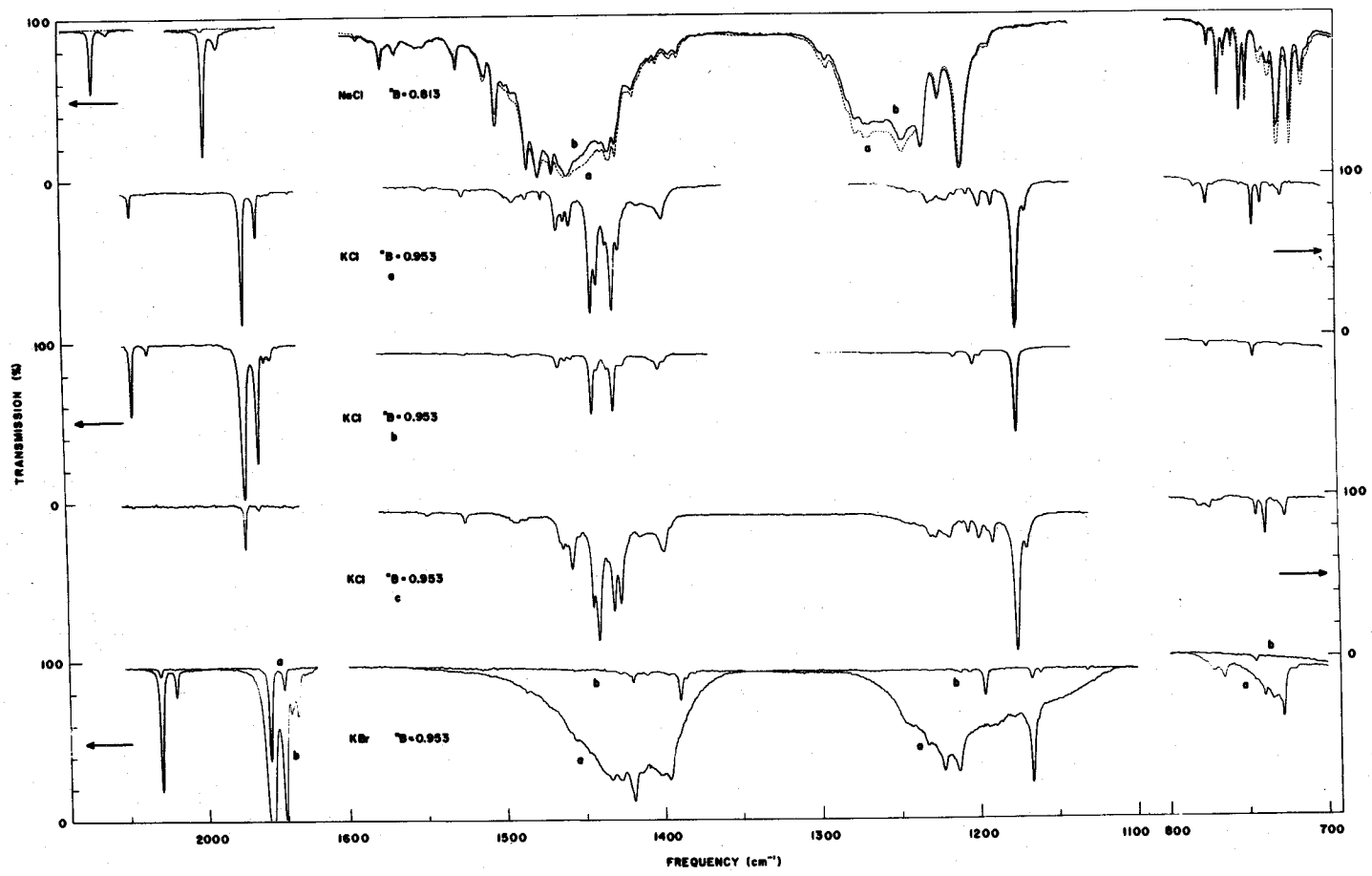
Figure 3. Spectra of boron containing species in a KCl
crystal with ^{11}B = .083 taken at T $\simeq$ 100°K
(700-1600 cm^{-1}) and T $\simeq$ 300°K (1940-
2050 cm^{-1}) which demonstrate the effect of
thermal history and boron concentration upon
the equilibria between species. The concen-
tration of boron increases from bottom to top.

a. (before quenching), b. (after quenching from
605°C), and c. (after annealing) denote the
thermal history of the crystal.

TRANSMISSION (%)

TOP
a

MIDDLE
a

MIDDLE
b

MIDDLE
c

BOTTOM
a

FREQUENCY (cm⁻¹)

23
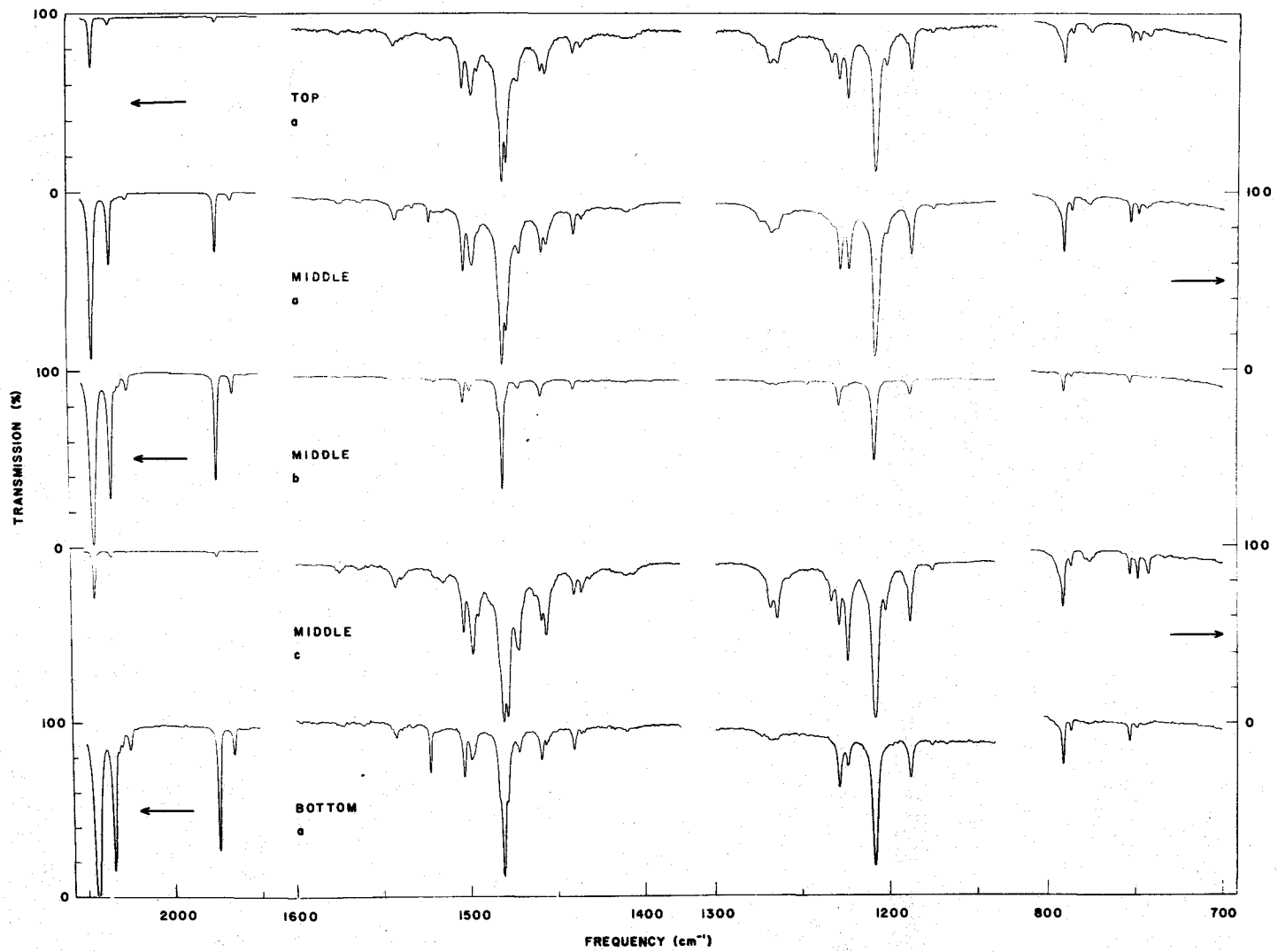
Figure 4. Spectra of boron containing species in KCl taken at $T \cong 100°$ K (700-1600 cm^{-1}) and $T \cong 300°$ K (1940-2050 cm^{-1}) which demonstrate the effect of thermal history and boron concentration upon the equilibria between species.

a. (before quenching), b. (after quenching from $605°$ C), and d. (after quenching from $710°$ C) denote the thermal history of a particular crystal.

a natural consequence if A is in solid solution because of spatial and electrostatic reasons which are considered below. If an impurity is in solid solution, the frequencies of the corresponding modes should decrease as the size of lattice is increased. This trend is shown in Tables 3 and 4 for one of the fundamentals of A. Furthermore, the sharpness of the features due to A and B suggest that they are in solid solution. For these reasons it is concluded that A and perhaps B are in solid solution.

Table 3. Interatomic distances in alkali halides.

	Anion-cation distances (42)	Calculated anion-anion distances
NaCl	2. 814	3. 980
KCl	3. 139	4. 439
KBr	3. 293	4. 657
CsI*	3. 950	4. 561

*CsCl structure

Table 4. ω_7 of species A.

	^{10}B	^{11}B
NaCl	1243	1210
KCl	1208	1175
KBr	1199	1166

Weir and Schroeder (41) have studied the infrared absorption spectra of anhydrous, crystalline, inorganic borates. Based on zinc metaborate which contains BO_4 tetrahedra with B-O distances of

1.48 $\overset{\circ}{A}$, they conclude only tetrahedrally coordinated boron would display its B-O stretching frequency in the 800-1100 cm^{-1} region. Because of a lack of stretching frequencies in this region with the exception of a weak doublet at 950 cm^{-1}, it has been concluded that the impurities being studied in this investigation do not contain BO_4 tetrahedra.

The fundamental ω_7 of species A, listed in Table 4, has at least four components whose intensities depend on the isotopic ratio of ^{10}B to ^{11}B. Some information can be obtained from this about the number of boron atoms in the molecule and the symmetry of the molecule. From the number of components it may be established that A must contain two or more boron atoms. Several models are considered in the next four sections.

<div align="center">Proposed Models for A</div>

Two Boron Atoms

Three isotopically different molecules which contain $2^{10}B$, $^{10}B + ^{11}B$, or $2^{11}B$ are possible; and the four lines may be accounted for if ω_7 is a degenerate mode which is split for the molecule containing $^{10}B + ^{11}B$. This is possible if there is either a threefold axis of symmetry or if the molecule has V_d symmetry. An example of the latter case is the hypothetical molecule shown in Figure 5, although such a molecule

is chemically very unlikely under these circumstances. The distance

between the two negatively charged oxygen atoms is about the same as

the halide-halide distance in an alkali halide crystal. Thus, this hy-

pothetical model might fit in an alkali halide lattice by replacing two

adjacent halide ions. This molecule contains two mutually perpendi-

cular BO_2^- groups and can be shown to have three vibrational funda-

mentals belonging to the E symmetry species which may be split into

B_1 and B_2 of the C_{2v} subgroup.
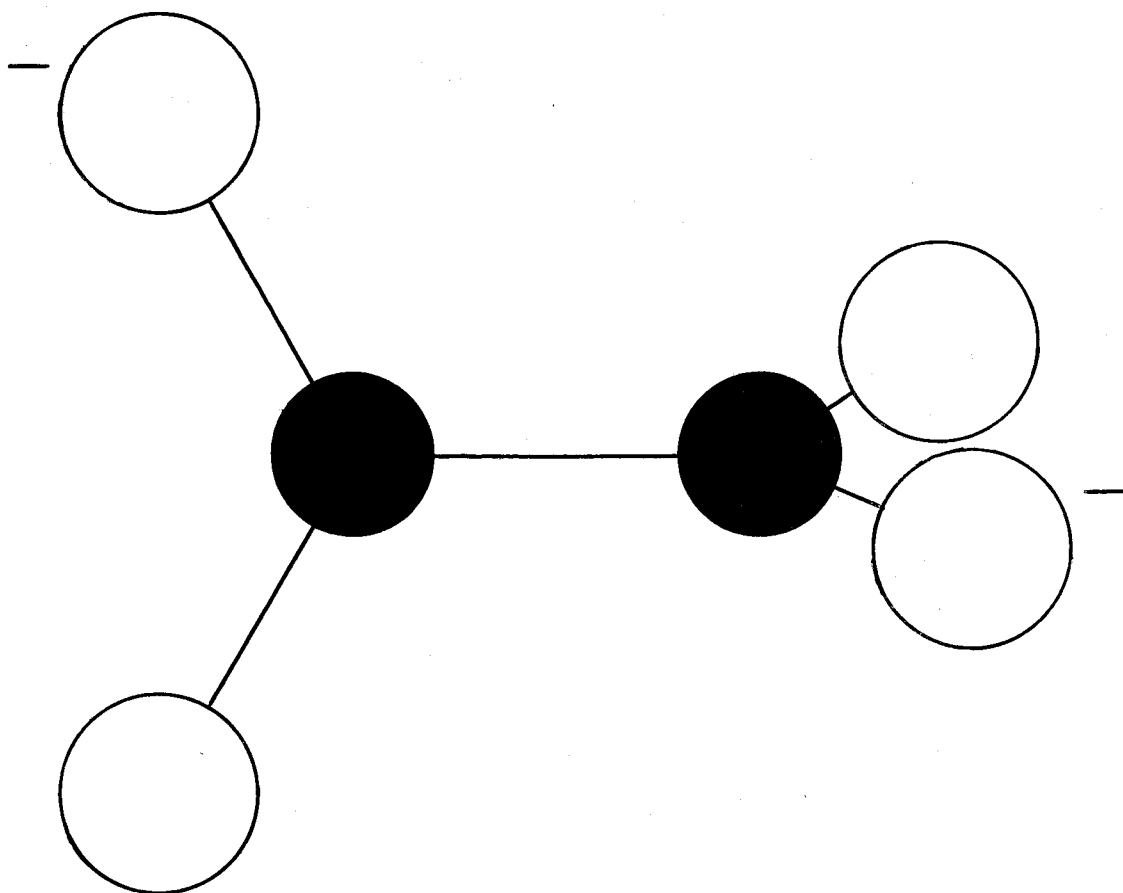
Figure 5. Hypothetical $(BO_2^-)_2$ ion which belongs to the V_d group.

A hypothetical molecule with a threefold axis, although unlikely, is one in which two BO_3 groups are held together through a boron-boron bond with three oxygen atoms and one boron atom at the corners of a tetrahedron and the remaining boron atom near the center. This structure may be described as two tetrahedra interposed at a corner. The details about the number of components are very similar to those of $(BO_2^-)_2$; however, these models are not able to predict the experimental intensities of ω_7 and the other fundamentals of A. This is shown qualitatively for ω_7 in Table 5.

Table 5. Comparison of experimental intensities of ω_7 with theoretical concentrations of the models containing two boron atoms.

	Theoretical				ω_7 in KCl			
$^{11}P^*$	$(^{11}P)^2$	$^{11}P^{10}P$	$^{11}P^{10}P$	$(^{10}P)^2$	1	2	3	4
.97	.94	.03	.03	.00	vs	vw	w	vw
.80	.64	.16	.16	.04	s	w	m	w
.50	.25	.25	.25	.25	vs	s	s	vs
.04	.00	.04	.04	.92	w	m	w	vs

$*^{11}P$ = probability that a boron atom is ^{11}B.

B_4O_6

Dunicz (12) recently proposed that this molecule has a cage structure in which four nonplanar BO_3 groups share oxygen atoms. He further proposes that the boron atoms may be coordinated to four external halide ions which are at the corners of a tetrahedron. It is

feasible that such a molecule could exist in an alkali halide lattice at the interstitial position (1/4, 1/4, 1/4) coordinated to four tetrahedral halide ions. Even though this is a large molecule compared to the amount of space available, it has been considered too.

This molecule has five isotopically different forms whose symmetry and the corresponding infrared active modes are given in Table 6.

Table 6. The isotopic forms of B_4O_6 and their symmetry.

Molecule	Symmetry	Symmetry species (IR active modes)
$4^{11}B$	T_d	F_2
$3^{11}B + {}^{10}B$	C_{3v}	$A_1 + E$
$2^{11}B + 2^{10}B$	C_{2v}	$A_1 + B_1 + B_2$
${}^{11}B + 3^{10}B$	C_{3v}	$A_1 + E$
$4^{10}B$	T_d	F_2

Internal symmetry coordinates of the symmetry species F_2

$$S_1 = 1/\sqrt{12}(3r_1 - r_2 - r_3 - r_4)$$

$$S_2 = 1/\sqrt{6}(2r_2 - r_3 - r_4)$$

$$S_3 = 1/\sqrt{2}(r_3 - r_4)$$

r_i = change in B(i) - X distance,

where X is a halide ion

Under C_{3v} symmetry if the boron corresponding to r_1 is

isotopically different, the appropriate internal symmetry coordinates (E) are similar to S_2 and S_3. Therefore E should occur at nearly the same frequency as F_2, but A_1 should be shifted a certain amount consistent with the Teller-Redlich product rule. The relative intensities expected and the possible positions are shown schematically in Figure 6 for two cases of splitting under C_{2v} symmetry. The first case is a zero order splitting in which no splitting is assumed, and the second case corresponds to an equal spacing between all three components. The experimental pattern of ω_7, four almost equally spaced components, and especially the concentration dependence cannot be explained by this model.

$(BO_2^-)_n$
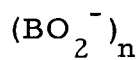
The infrared spectra of nujol mulls of CaB_2O_4 published by Goubeau and Hummel (24) and observed in this investigation are in many respects similar to the one corresponding to species A. The crystal structure was determined by Zachariasen and Ziegler (44, 46, 47) to be orthorhombic and to contain the polymer $(BO_2^-)_n$. This polymer is a nearly planar chain of BO_3 groups which share one oxygen as shown in Figure 7. The distance between two adjacent negatively charged oxygen atoms is approximately equal to the halide-halide distance in an alkali halide crystal. Therefore this large polymer might possibly fit in the lattice if the negatively charged oxygen

ZERO ORDER   EQUAL SPACING

4 ^{11}B

3 ^{11}B + ^{10}B

2 ^{11}B + 2 ^{10}B

^{11}B + 3 ^{10}B

4 ^{10}B

SUM
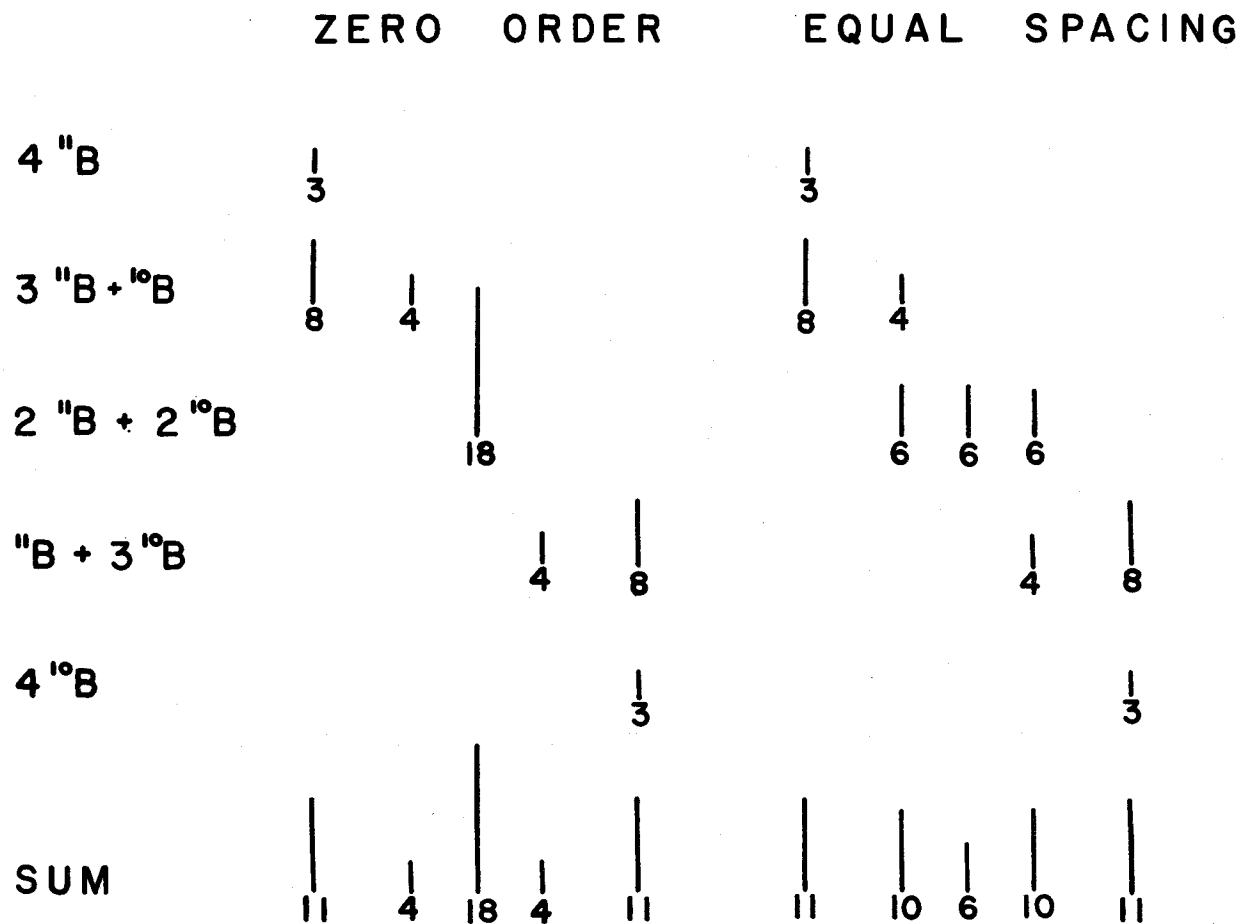
Figure 6. Isotopic components of a triply degenerate mode (F_2) of B_4O_6 indicating proposed positions of the members of an isotopic component which result from a reduction in the symmetry due to the appropriate isotopic perturbation. ^{11}P = 0.5.

32
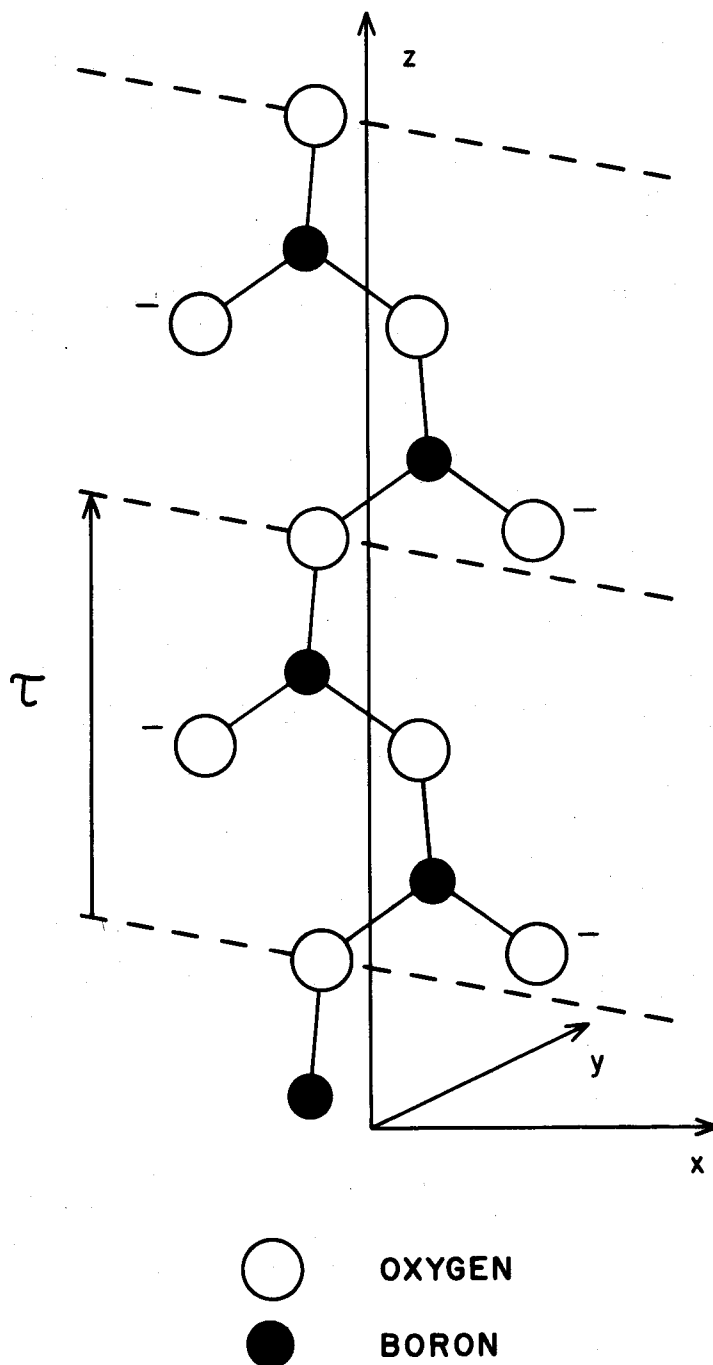
Figure 7. The structure of $(BO_2^-)_n$ from calcium metaborate according to Zachariasen (44). τ is the primitive translation vector which defines the unit cell in this one dimensional lattice.

atoms replace two parallel rows of halide ions such that τ is parallel to a $<110>$ direction and a normal to the plane of the molecule is in a $<111>$ direction.

The unit cell consists of $(BO_2^-)_2$, and if it is planar the following symmetry operations are present; E, σ_{xz}, $[C_2; \tau/2]$, and $[\sigma_{yz}; \tau/2]$. Hence $(BO_2^-)_n$ belongs to a group which is isomorphic to C_{2v}. A normal coordinate analysis using several simplifying assumptions such as separation of high and low frequencies, stretching and bending modes respectively, predicts stretching frequencies which agree to some extent with the experimental ones. However, this model will not account for the positions of the isotopic components of the modes which have been ascribed to species A. Decius, Malan, and Thompson (7, 10) have dealt with similar problems involving intermolecular coupling between nitrates and between carbonates which are arranged in a chain in the aragonite structure. Their calculations predict that the frequencies due to isotopically pure chains will be either larger or smaller, depending upon the sign of the coupling constant in the F matrix, than those due to the corresponding sequence of slightly impure chains. However, in this investigation the mixed isotope components are between those of the two pure isotopes. If a chain has a threefold axis of symmetry or belongs to the group V_d, then the isotopic components of a doubly degenerate mode would possibly fit such a pattern. No such polymer is

known to exist or is physically imaginable.

Trimer of Metaborate, $(BO_2^-)_3$

The infrared spectra of $K_3(BO_2)_3$ and $Na_3(BO_2)_3$ (24, 28) in mineral oil mulls and in pressed disks of alkali halides are quite similar to those of species A. The trimer has four different isotopic forms and consequently each fundamental should have at least four components. The doubly degenerate fundamentals are split by the reduction in symmetry from D_{3h} to C_{2v} for the molecules containing one nonequivalent boron isotope. The four components of ω_7 and their intensities may be accounted for if the six components which result from the removal of the degeneracy under C_{2v} symmetry overlap in the manner shown schematically in Figure 8. A qualitative comparison of experimental intensities and theoretical concentrations is given in Table 7.

Table 7. Comparison of experimental intensities of ω_7 with theoretical concentration of $(BO_2^-)_3$.

| Theoretical | | | | | ω_7 in KCl | | | |
| $(^{11}P)^3 +$ | | | $(^{10}P)^3 +$ | | | | | |
^{11}P	$3/2(^{11}P)^2(^{10}P)$	$3/2(^{10}P)^2(^{11}P)$	$3/2(^{11}P)^2(^{10}P)$	$3/2(^{10}P)^2(^{11}P)$	1	2	3	4
.97	.96	.00	.04	.00	vs	vw	w	vw
.80	.72	.04	.18	.05	s	w	m	w
.50	.31	.19	.19	.31	vs	s	s	vs
.04	.00	.06	.00	.94	w	m	w	vs
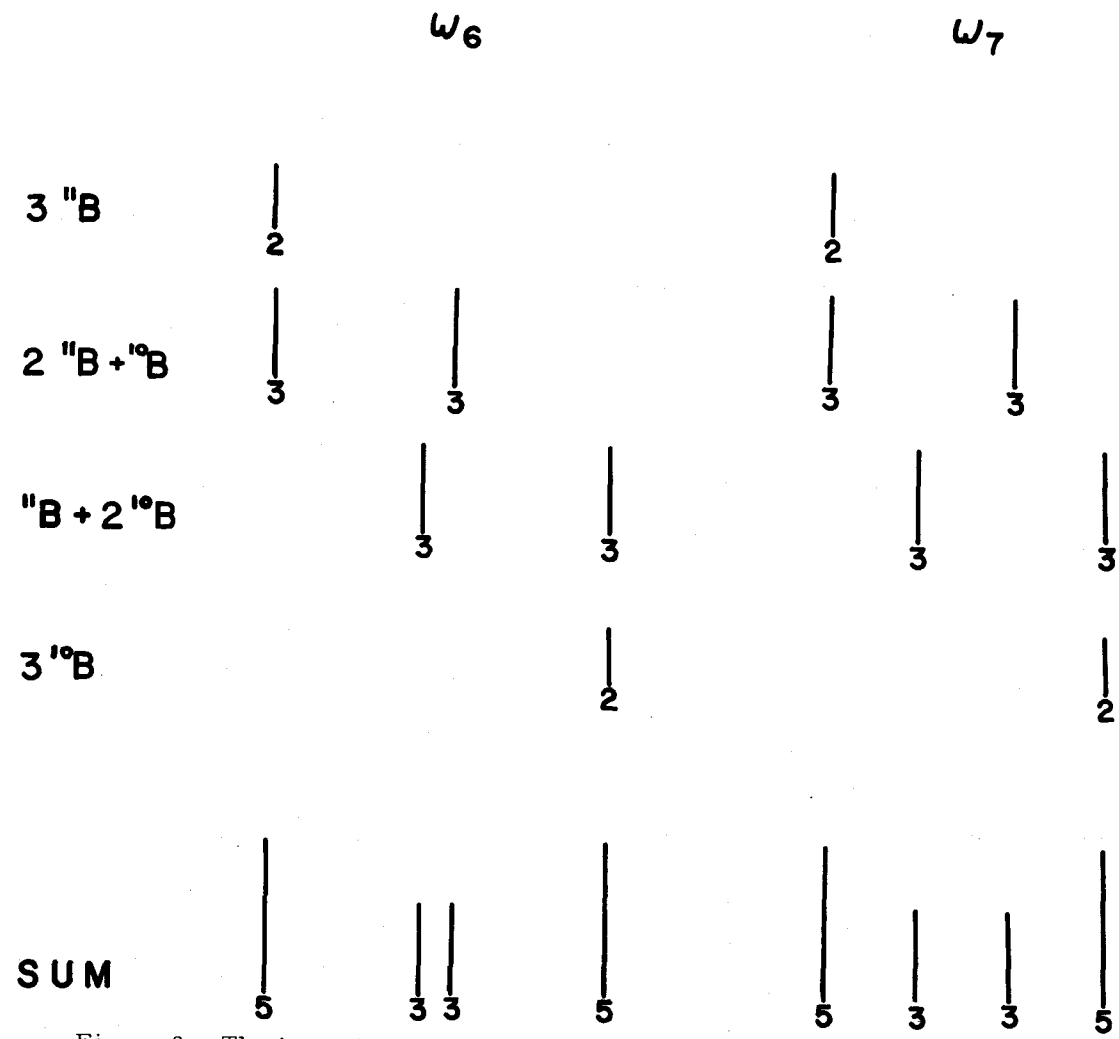
Figure 8. The isotopic components of ω_6 and ω_7 of the metaborate trimer when $^{11}P = {}^{10}P = 0.5$.

The trimer ion belongs to the D_{3h} group, and its planar struc-

ture in $K_3(BO_2)_3$ according to Zachariasen is shown in Figure 9.
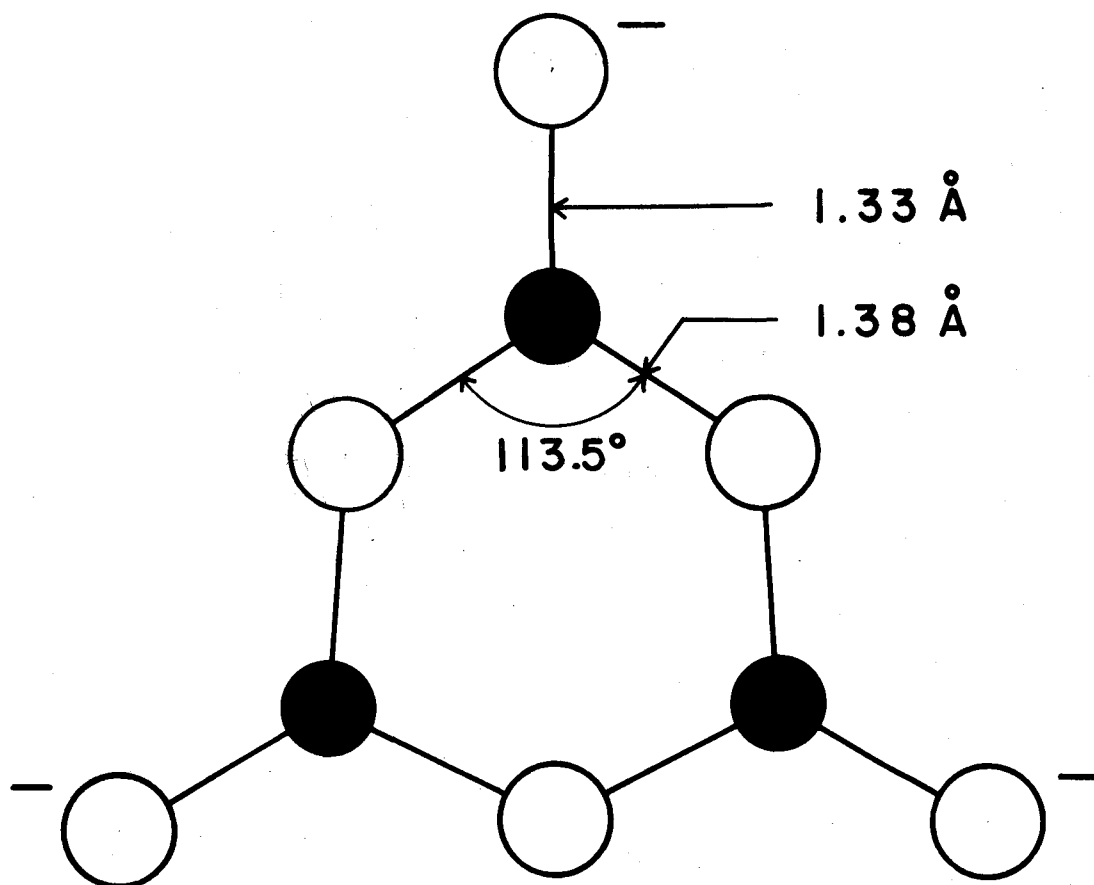
Figure 9.   The metaborate trimer in $K_3(BO_2)_3$ according to
Zachariasen (45).

The trimer in the potassium salt has a ring B-O distance of

1.38 Å, an external B-O⁻ distance of 1.33 Å, and an interior ring

O-B-O angle of 113.5°.   Whereas these bond lengths in the sodium

salt are reported by Marezio et al. (30) to be 1.433 Å and 1.280 Å

respectively.   It is feasible that the trimer ion fits in an alkali halide

lattice by replacing three next nearest neighbor halide ions which form an equilateral triangle. The plane of the trimer would then be in a (111) plane in the crystal as shown in Figure 10.

Using the dimensions for the trimer in the potassium salt, the O^--O^- distance was calculated to be 4.74 $\overset{\circ}{A}$, and the anion-anion distances for NaCl, KCl, KBr, and CsI have been listed in Table 3. Although the impurity fits best in KCl, a consideration of the anion-anion distances suggests that KBr should be the best host. This argument assumes that the three negative charges are on the exterior oxygens which is not altogether true. The ring B-O distance is longer than the exterior B-O^- distance; hence the exterior B-O^- bond must have more double bond character. Thus the actual structure of the trimer ion must be somewhere between the two resonance structures shown in Figure 11.

Dingle (11) determined the bond order of π electrons in several boron-oxygen compounds using the standard Hückel-type analysis including the ω-technique. Some of these calculated bond orders and published bond lengths are given in Table 8. By interpolation the bond order of the exterior B-O^- and interior B-O bonds for the potassium salt should be approximately 0.54 and 0.45. Therefore, the oxygen exterior to the ring shares two π electrons with the boron atom approximately half of the time. The negative charge should, on the average, be situated along the exterior B-O bond about 1/4 of the bond
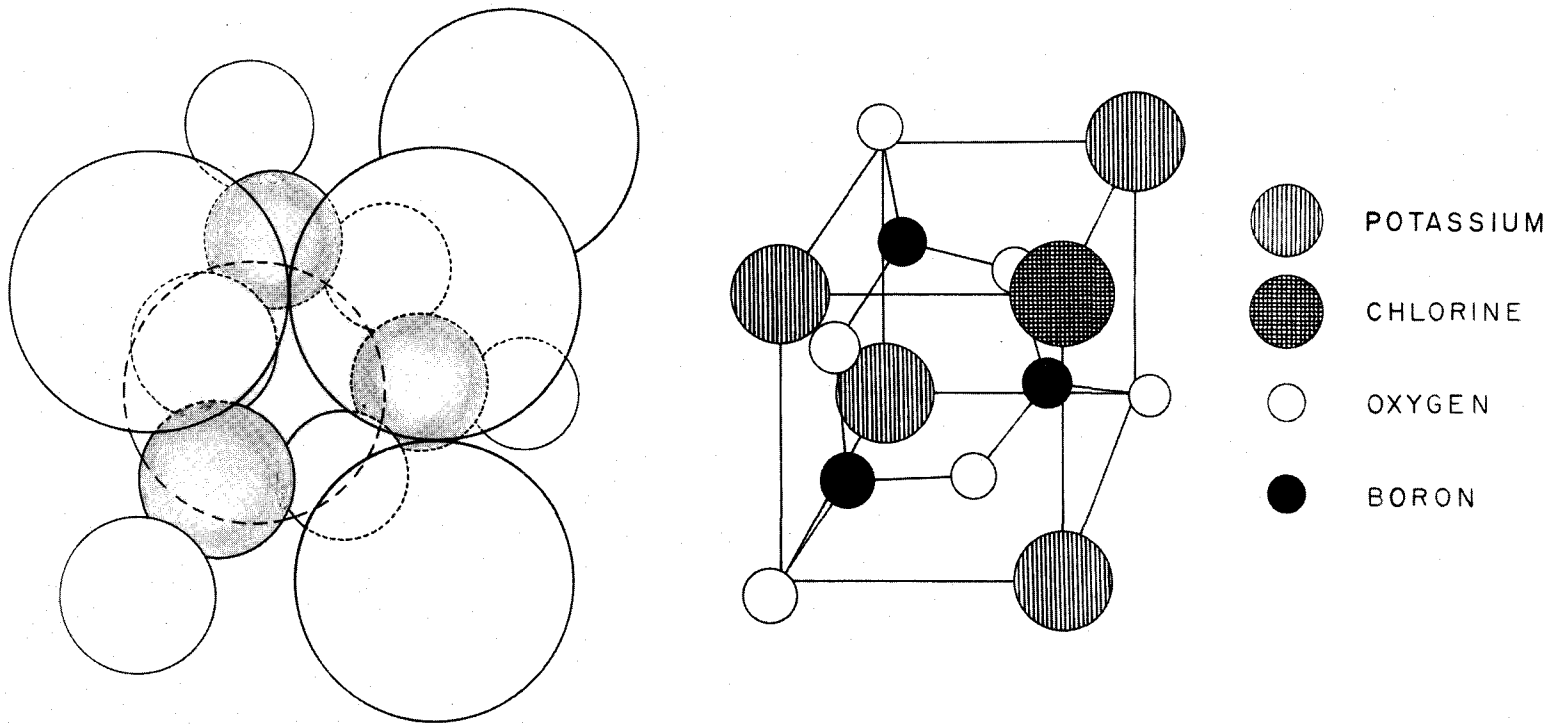
Figure 10. The metaborate trimer, $(BO_2^-)_3$, in solid solution in the KCl lattice.

length from the oxygen atom. Several distances between two negative charges have been calculated and are tabulated in Table 9 assuming specified distances between the boron atom and negative charge. If the distance between the boron atom and the negative charge is 1.00-1.15 Å which is consistent with the bond order calculations, then the electrostatic energy required to introduce the trimer into the lattice would be a minimum for either KCl or NaCl.
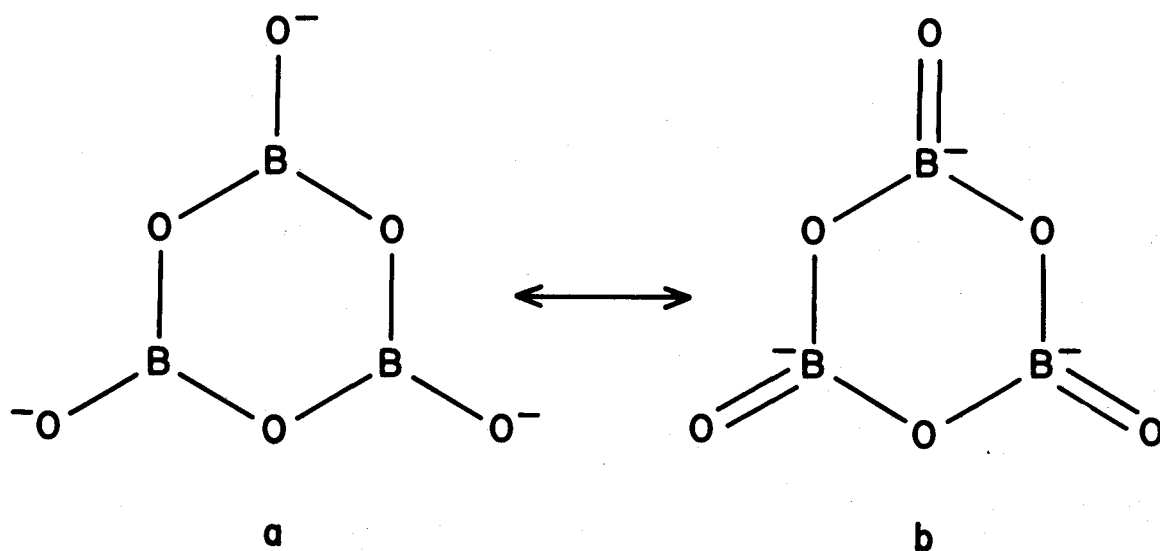
Figure 11. Two resonance structures of the metaborate trimer.

Table 8. Bond order of π electrons in boron-oxygen compounds according to Dingle (11).

Molecule	Bond	Bond length (Angstroms)	References	Bond order	
				Simple theory	ω-technique
$B_3O_6^{-3}$	BO-B	1.433	30	...	0.372
BO_3^{-3}	OB-O	1.35		0.555	0.503
$B_3O_6^{-3}$	B-O$^-$	1.28	30	...	0.599

Table 9. Distance between two negative charges in the
metaborate trimer.

Distance between boron and negative charge	Distance between two negative charges
1. 00 Å	4. 16 Å
1. 10 Å	4. 34 Å
1. 15 Å	4. 43 Å
1. 33 Å	4. 74 Å

Spatial considerations alone predict that the solubility of the
trimer should increase as the size of the lattice and the ratio of anion
to cation radii increase. Thus, for spatial reasons KBr should be
the best host lattice; however for this model, in light of the electro-
static arguments, it is reasonable to expect KCl to be the best host.
In this model the ring of the cyclic trimer fits in an interstitial posi-
tion with the three ring oxygens and center of the ring situated near
(1/4, 1/4, 0) and (1/6, 1/6, 1/6) respectively. There are three K^+
ions at (1/2, 1/2, 0) and one K^+ at (0, 0, 0) which lie directly above
and below the ring. The calculated positions of the atoms of the un-
distorted trimer assuming that the distance from the boron atom to
the special lattice sites (1/2, 0, 0) is 1. 15 Å, are given in Table 10
as well as the distances between these atoms and nearby K^+ ions.

The amount of space available can now be compared with appro-
priate dimensions of this model which have been approximated with
the aid of ionic radii recently published by Fumi and Tosi (21). These

ionic radii in addition to the ionic radius of $O^=$ calculated from the in-
teratomic distance of 2. 00 Å in Li_2O, are listed in Table 11. To a
first approximation the ionic radius of $O^=$ may be used as the radius
of the oxygen in the trimer. However, the oxygen radii which are
orientated toward the K^+ ions should be smaller than the ionic radius
because of localization of bonding σ and π electrons. The localiza-
tion of nearly one π electron per B-O bond is expected to cause
the greatest decrease in the radii in the directions of interest. If
these radii are assumed to be 0. 7 Å, the sums of appropriate radii
are in good agreement with the distances between the trimer atoms
and K^+ ions. The radius of boron is assumed to be the same; there
is even less information about the ionic radius of boron while cova-
lently bonded. If the effective radii are larger than 0. 7 Å, the cor-
responding electronic clouds would be compressed or more likely the
trimer and lattice would be distorted. Even if it does not occur for
this reason, a puckering of the ring is expected due to the expected
discrepancy between the distance from the K^+ at (0, 0, 0) to the cen-
ter of the ring at (1/6, 1/6, 1/6), and the sum of the ionic radius of the
K^+ and the half-thickness of the ring at the center. The bonding π
electrons which are localized along B-O bonds project above and be-
low the plane of the ring. Hence, the half-thickness of the ring at the
center should be less than the radii of the atoms in the ring. In light
of this, the half-thickness of the ring is assumed to be . 1 Å less than

the radii of the boron and oxygen atoms resulting in 2.1 Å for the appropriate sum in the most favorable case as compared to 1.8 Å, the distance between (0, 0, 0) and (1/6, 1/6, 1/6).

Table 10. Positions of undistorted trimer atoms in the KCl lattice.

O^-	(-.012, .524, -.012)
O	(.255, -.010, .255)
B	(.075, .350, .075)

Interatomic distances between trimer and KCl lattice

d	O^-	O	B
K (0, 1/2, 1/2)	3.07		2.87
K (1/2, 0, 1/2)		2.18	
K (0, 0, 0)	3.29	2.26	2.30

Table 11. Ionic radii according to Fumi and Tosi (26).

	Ionic radii Å
K^+	1.54
Cl^-	1.60
$*Li^+$	.86-1.00
$O^=$	1.14-1.00

* Represents the range found in four lithium halides.

Because of the C_{3v} symmetry of the three K^+ ions above the ring and the one K^+ below it, any perturbation of the trimer would

lower the symmetry from D_{3h} to C_{3v}. A distortion of the lattice in the vicinity of this impurity would be expected to take the form of larger lattice constants while the symmetry of the site occupied by the trimer should be C_{3v} just as in the unperturbed case. Such a distortion seemed to be present, for it was evident that the single crystals which contained the impurities were strained to a greater extent than pure single crystals grown by the same method.

CsI was doped with H_3BO_3 and most of the HI and H_2O formed was removed by evacuation. However no infrared absorption bands were observed. This is consistent with the above model because in the CsI lattice, which has the CsCl structure, the anion lattice sites form squares rather than the necessary equilateral triangles.

In light of the foregoing discussion the metaborate trimer ion which replaces three next nearest neighbor halide ions is considered the best model.

Proposed Model for C

The impurity which has been called species C is proposed to be the appropriate salt of the trimer ion in a second phase. This is based on the spectrum of $Na_3(BO_2)_3$ observed by Goubeau and Hummel (24) and on the spectra observed by Hisatsune and Suarez (28). These experimental data are summarized for the sodium salt in Table 12. In the present investigation there is more of this impurity in

NaCl and KBr than in KCl; see Figure 2. The lines assigned to $K_3(BO_2)_3$ in KCl and KBr, and the data of Hisatsune and Suarez are given in Table 13. Their assignment for KBr, being more complete, has been used rather than the assignment for KCl. Their experimental frequencies for KCl and KBr are the same within experimental error; see Table 2.

Table 12. Some fundamentals of $Na_3(BO_2)_3$. (cm^{-1})

Goubeau and Hummel		Hisatsune and Suarez T $\cong$ 300° K		Present work T $\cong$ 100° K	
ω_6	1450 vs, vb	ω_6	1466	ω_6	1458 b
	1425 vs, vb		1436		1432 b
ω_7	1255 s, b	ω_7	1264	ω_7	1268 b
	1227 s, b		1241		1246 b
ω_8	720 w	ω_{11}	724	ω_{11}	720. 5
	702 m		708		703. 4

The crystal structure of potassium and sodium metaborate has been determined by Zachariasen (45) and Fang (14) respectively to be rhombohedral with the space group $R\bar{3}c$ (D_{3d}^6). There are two $K_3(B_3O_6)$ or $Na_3(B_3O_6)$ molecules per unit cell, and the $(BO_2^-)_3$ groups occupy sites having D_3 symmetry. The number of internal modes, their symmetry species, and spectral activity may be obtained by means of correlation diagrams which are given in Figure 12. Because A_{2u} and E_u modes are infrared active for the D_{3d} group; ω_4, ω_5, ω_{13}, and ω_{14} should become infrared active in the crystal.

Table 13. Some fundamentals of $K_3(BO_2)_3$. (cm^{-1})

	Hisatsune and Suarez $T \simeq 300°K$				Present work in KCl $T \simeq 100°K$				Present work in KBr $T \simeq 100°K$	
	B^{nat}	B^{syn}	^{11}B	^{10}B	B^{nat}	B^{syn}	^{11}B	^{10}B	^{11}B	^{10}B
ω_6	1405 vs	1406 vs	1400 vs	1460 vs	1401 m	1405 m	1399 m	a	1400 vs	1470 vs
ω_7	1225 s	1233 s	1222 vs	1238 s	1225 b, m	1225 b	1220 b		1228 vs	1232 s
	1249 s	1257 vs	1247 s	1265 vs	1245 b, w	1255 b, m		1265 m	1250 s	1260 s
ω_{11}	734 s	736 s	728 s	754 s	726 w	728 vw	726.5vw	743 w	728 s	749 m
	746 s				732 w	732 w	732.6 vw			

a $= $ obscured

$B^{nat} = $ natural abundance

$B^{syn} = 50\%$ ^{11}B
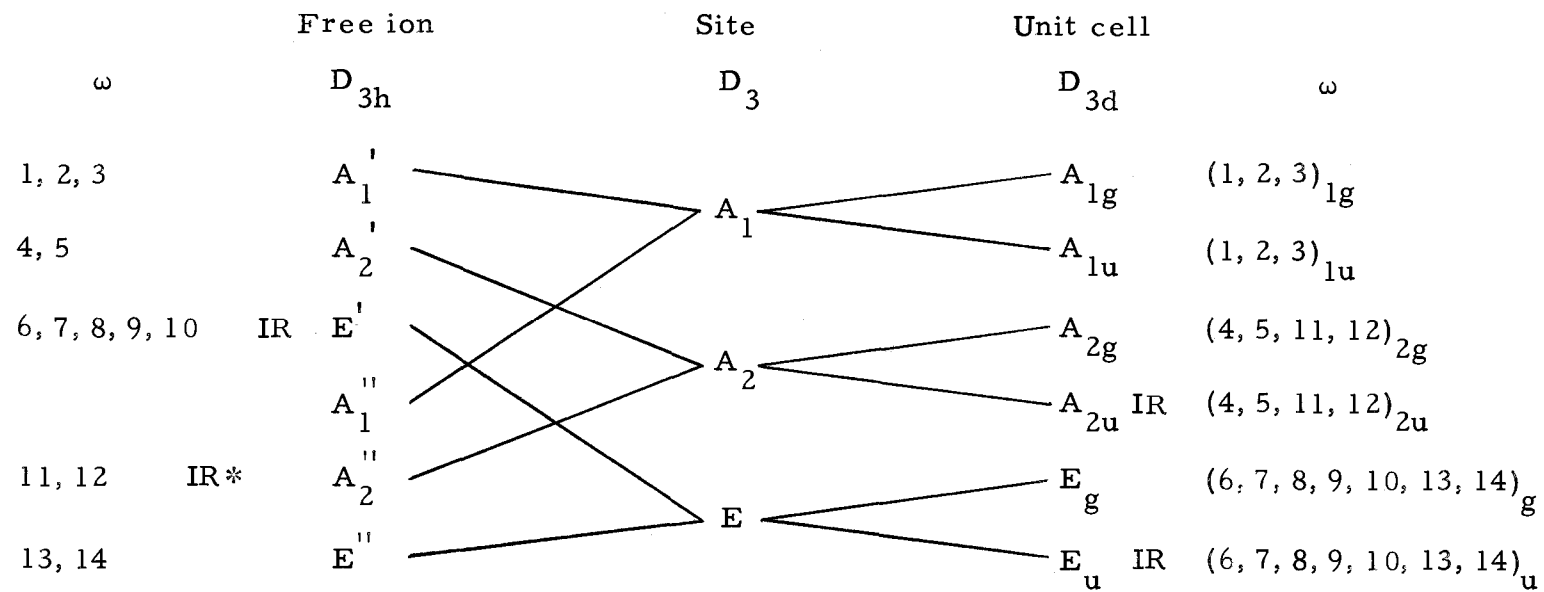
Figure 12. Correlation diagrams and spectral activity corresponding to the metaborate trimer as a free ion and in the rhombohedral unit cell of $K_3(BO_2)_3$ or $Na_3(BO_2)_3$.

There is a further complication which must be considered. If adjacent trimer ions are isotopically nonequivalent, then a weak interaction would result. There should, therefore, be more components than originally anticipated, and the components due to the trimer with equivalent borons should become weaker when mixtures of boron isotopes are used. This is found to be the case. If adjacent C_{2v} trimer ions are to be isotopically equivalent, in addition to containing the same number of ^{10}B and ^{11}B atoms, the nonequivalent boron atom in one trimer ion must occupy the same position as the corresponding boron atom in the adjacent trimer ion. Therefore a large number of modes are expected which may account for the broad, almost polymer-like bands.

Light Scattering Evidence of a Second Phase

The bands observed by Hisatsune and Suarez (28), previously attributed to a second phase, and the good agreement between their observations and those in NaCl and KBr in this investigation suggest that a second phase is present. The width of these bands is also evidence of a second phase. In order to confirm the presence of a second phase, scattering experiments using visible light were performed. Defect scattering was observed in NaCl and KBr doped with $NaBO_2$ and KBO_2 respectively with an ultramicroscope, and photomicrographs were taken and are shown in Figure 13. It appears that one

Figure 13.   Light scattering observed by means of an
             ultramicroscope.

a. doped KBr   e. pure KBr
b. doped NaCl   f. pure NaCl
c. doped KBr   g. doped KCl
d. doped NaCl   h. pure KCl
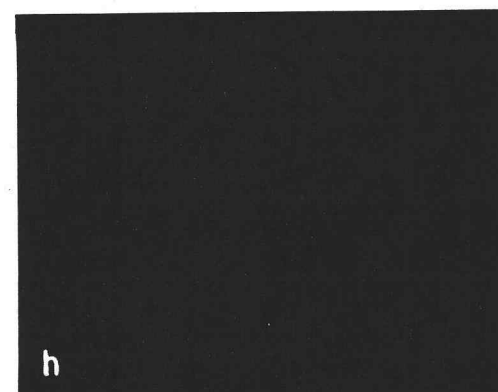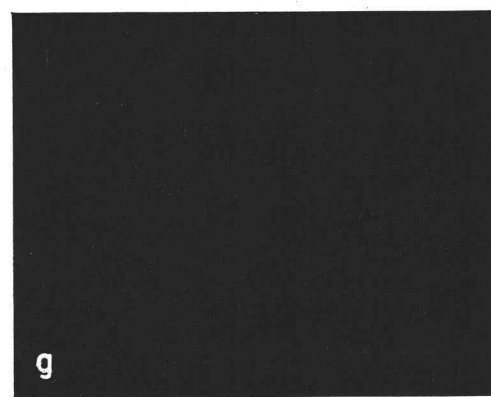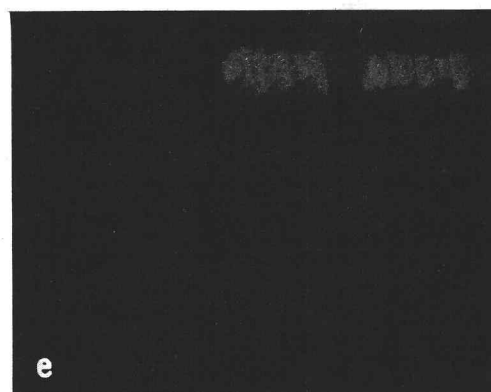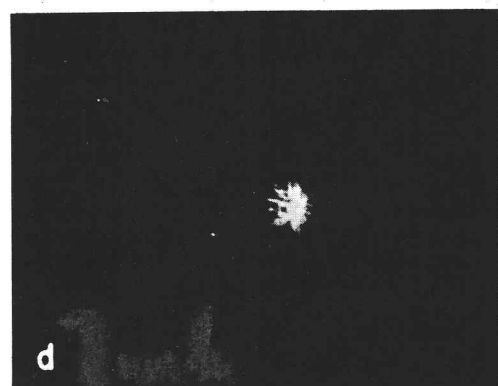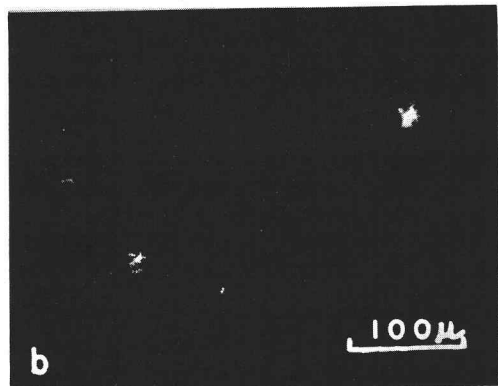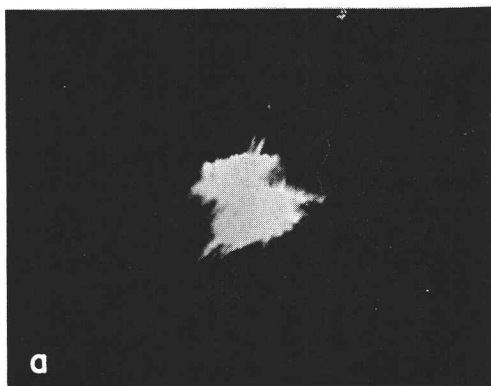
should be able to estimate the size of the defects; however, the microscope was focused in order to maximize the scattered light and therefore the microscope was not, in general, focused on the defects but on the light scattered from the defect. Aside from a few large clusters of defects the size of the scattered light became relatively much smaller when the microscope was focused on an individual scattering center. Bansigir and Schneider (2) conducted direct microscopic studies and measurements of the optical scattering spectrum of relatively pure and doped alkali halide crystals. Using the Mie theory they calculated the radii of their equivalent scattering spheres to be of the order of 1600 $\overset{\circ}{A}$.

In the present investigation the amount of defect scattering was measured by means of a recording polarization spectrometer (13). The incident light was vertically polarized and designated E, and the vertically and horizontally polarized components, E and B respectively, of the scattered light were measured perpendicular to the incident light. The EB component is a measure of the scattered light which has been depolarized by the defects and by things such as surfaces, whereas the EE component is a measure of light scatter from surface imperfections. Consequently, the ratio EB/EE is related to the amount of light which has been depolarized by defects and therefore to the number and size of the defects. The EB/EE ratio is tabulated in Table 14 for several different crystals which were grown in this

laboratory by the Stockbarger method except for the pure KBr crystal
which is a Harshaw crystal. This behavior is typical for Harshaw
crystals due to very small bubbles and other defects introduced during
the growing process. Therefore, the amount of defect scattering in
doped NaCl and KBr is significant, whereas the defect scattering in
doped KCl is much smaller.

Table 14. Light scattering in alkali halides.

		EB/EE	Ratio of doped to pure
KCl	pure	.26	1.2
KCl	doped	.32	
NaCl	pure	.27	1.8
NaCl	doped	.49	
*KBr	pure	.46	1.0
KBr	doped	.48	

* Harshaw crystal

In a recent investigation by Squire and Zamecki (38) the optical
birefringence in pure single crystals of KCl and LiF has been studied.
The crystals used in their study typically contained some 10^6 disloca-
tions per cm^2 which arise during the growth from the melt.

> Unless the temperature gradient across the liquid-to-
> solid interface is kept very uniform, a stress is gener-
> ated which is relieved by the formation of dislocations.
> These dislocations are preferentially oriented in the
> crystal because the temperature gradient which is not
> uniform within the furnace has an orientation.

Their results using polarized light demonstrated that a majority of the

defects which produce the optical anisotropy may be linked with the

<100> direction. Adair, Sharp, and Squire (1) observed that these

same crystals have a small paramagnetic, uniaxial anisotropy by

means of a delicate torsion pendulum technique and assigned the mag-

netic centers to a great number of dislocations orientated along the

<100> direction. In addition, two recent optical studies on alkali hal-

ides support the above evidence for dislocations acting as scattering

centers. Plint and Watson (36) reported light scattering from charged

dislocations in KCl:Pb whose intensity has fourfold symmetry when

the crystal is rotated about an axis parallel to the <100> direction at

23 rev/sec. The scattered light was observed at 90° to the incident

light which was incident upon the (100) plane using a photomultiplier and

an amplifier tuned to 92 and 184 cps. The ratio of the signals at the

two frequencies gives some information on the shape of the centers.

They attributed the scattering centers to charged dislocations which

have an effective diameter of 100 $\overset{\circ}{A}$, have an approximate length of

10, 000 $\overset{\circ}{A}$, and may be orientated in the <100> direction. Taurel and

Girard-Nottin (40) observed light scattering in single crystals of sodi-

um chloride, and the intensity was found to have fourfold symmetry as

the crystal was rotated in a manner similar to that of Plint and Wat-

son. The authors attributed the scattering centers to orientated pre-

cipitates which decorate dislocation lines.

Many dislocations are expected in the crystals grown during this

investigation because of the nonuniform temperature gradient across the liquid-to-solid interface. Therefore, it seems reasonable to assign the defects which are responsible for light scattering to precipitates along dislocation lines. It is evident from the photomicrographs that the defects tend to lie along what seem to be crystalline axis, particularly in the larger clusters of defects. When the doped crystals were quenched from near the melting temperature to near the boiling point of liquid nitrogen, the intensities of the broad bands became smaller. The size of this attenuation increased for the series NaCl, KCl, and KBr from a slight attenuation in NaCl to an apparently complete removal of these bands in KBr. Moreover, no scattering centers were observed with the ultramicroscope in the KBr crystal after quenching. This is good evidence that the broad infrared bands and the light scattering are both due to the potassium and sodium salts of the metaborate trimer.

Proposed Model for B

The spectral information on species B is quite complex, and has thus far defied a complete interpretation. The infrared bands occur near the fundamental and combination bands of the trimer, and their intensities vary independently of the trimer band intensities as the concentration of boron and as the thermal history are varied. Most of the bands of B as well as the corresponding trimer bands are

listed in Table 15 for the molecules containing $3^{10}B$ and $3^{11}B$. The assignment is much less complete for the molecules containing a mixture of boron isotopes due to the much greater complexity.

Species B is favored as the concentration of boron becomes larger and when the crystal is annealed slowly compared to a rapid quench. That both of these conditions favor larger molecules coupled with the proximity of the infrared bands of the trimer and species B suggest that B contains trimer ions which are somehow associated. These trimer ions could share an exterior oxygen or they might merely be on adjacent sites. Interactions between adjacent trimer ions have been discussed in the previous section, and they are theoretically capable of producing the observed perturbations on the vibrational modes of the trimer.

Some of these perturbed modes are more intense than other perturbed modes relative to their adjacent trimer modes. This may be explained using this model as follows. The size of the interaction and consequently the resulting normal coordinate depends upon the unperturbed motion or the original normal coordinate and the orientation of the two trimer ions. The integrated intensity, in turn, is related to the perturbed normal coordinate, Q_k, according to the expression

$$I_k = \left(\frac{\partial \mu_x}{\partial Q_k}\right)_0^2 + \left(\frac{\partial \mu_y}{\partial Q_k}\right)_0^2 + \left(\frac{\partial \mu_z}{\partial Q_k}\right)_0^2 = \left(\frac{\partial \mu}{\partial Q_k}\right)_0 \cdot \left(\frac{\partial \mu}{\partial Q_k}\right)_0 \qquad (3\text{-}1)$$

in which μ_x, μ_y and μ_z are components of the dipole moment. For these reasons species B is tentatively attributed to interation between trimer ions.

The Monomer of Metaborate and Boron Isotope Ratios

The metaborate monomer is a symmetrical linear ion which is isoelectronic with carbon dioxide. It was first observed in commercial NaCl by McDonald (31) and later studied in KCl and KBr by Morgan and Staats (32). The latter investigators observed the combination band $\omega_2 + \omega_3 - \omega_2$ in addition to the fundamentals ω_2 and ω_3. The initial state corresponding to the transition $\omega_2 + \omega_3 - \omega_2$ is Π_u as shown in Figure 14, and the population of this state is

$$2e^{-h\omega_2 c/kT} \tag{3-2}$$

times the number in the ground state Σ_g^+ (00° 0).

To a first approximation when calculating the number of $\omega_2 + \omega_3 - \omega_2$ transitions relative to ω_3, the same Boltzmann factor can be employed. This is very useful when calculating the relative amounts of isotopic boron in highly enriched boron samples because of the large errors which are normally present when comparing largely different absorbances. At room temperature this Boltzmann factor is about .10 which allows a favorable comparison between $\omega_2 + \omega_3 - \omega_2$

Table 15. Trimer fundamentals and trimer interaction bands in KCl at $\simeq 100°K.$ (cm^{-1})

	Trimer				Trimer interaction			
	$3^{11}B$	$2^{11}B+^{10}B$	$^{11}B+2^{10}B$	$3^{10}B$	$3^{11}B$	$2^{11}B+^{10}B$	$^{11}B+2^{10}B$	$3^{10}B$
ω_{11}	773.5	781.1	786.6	791.1	770 w			
ω_7	1175.2	1175.9 1198.7	1188.3 1207.9	1208.8	1169 w 1190.6 m 1206.2 m	1195 sh	1200 sh	1202.5 w 1224.3 m 1233.6 mw
ω_6	1430.6	1430.8 1460.8	1459.4 1480.8	1481.8	1426.5 m 1440.0 s 1457.5 m 1463.4 w	1452	1457	1472 w 1479 s 1495 w 1499 w

Figure 14. The fundamental ω_3 and combination $\omega_2 + \omega_3 - \omega_2$ of the metaborate monomer.

of the enriched isotope and ω_3 of the other isotope. Values of .039 and .027 were obtained by this method for ^{10}B and ^{11}B in enriched samples, and the respective isotopic contents according to the manufacturer are .040 and .026.

It may easily be shown that

$$\sum_k \frac{I_k}{(\omega_k)^2} \tag{3-3}$$

is an isotopic invariant where I is the integrated intensity and the sum is carried out over the k normal modes which belong to the symmetry species of interest; see for example Wilson, Decius and Cross (43). Therefore, the absorption coefficient which is proportional to the integrated intensity is larger for the isotopic component which occurs at a higher frequency. Since ω_3 is the only fundamental of BO_2^- which corresponds to the Σ_u^+ symmetry species, the relative isotopic absorption coefficients can be calculated. The reported isotopic compositions have accordingly been corrected, but those used in predicting absorbances of the fundamentals of the trimer were not, becuase similar but unknown corrections would have to be applied to the experimental absorbances.

This combination band may also be used to determine the temperature of the crystal by means of the temperature dependence of the Boltzmann factor given in Equation 3-2.

Equilibria Between Impurities

The equilibria that exist between the impurities depend upon the lattice, concentration of boron, and thermal history; and they are discussed in light of the proposed models. As the total concentration of $NaBO_2$ becomes larger within the same NaCl crystal, the increase in concentration of $Na_3(BO_2)_3$ is greater than that of the trimer in solid solution. Conversely, the concentration of monomer actually decreases as the concentration of boron increases within the same crystal. Upon quenching, the amount of precipitate decreased slightly, the trimer remained unchanged within experimental error, but the accompanying increase in the monomer was apparently greater than anticipated as may be seen in Figure 2. It should be borne in mind that the removal of each trimer ion results in three monomer ions and that the monomer lines are much narrower. Thus, the increase in monomer ions merely appears to be greater than anticipated.

The dependence upon boron concentration is very similar in KCl for the monomer, trimer, trimer interaction, and $K_3(BO_3)_3$ and is shown for the first three in Table 16 and in Figures 3 and 4 for typical crystals. The numbers in Table 16 should be considered only as approximate indications of relative changes in each of the three impurities. The boron concentration in one crystal was determined colorimetrically to be four times greater in a sample near the top compared

to near the bottom. In some very dilute samples the trimer interaction bands were almost completely missing.

Table 16. Relative concentrations of the monomer, trimer, and trimer interaction in a KCl crystal.

	Monomer	Trimer	Trimer interaction
Top	1	6	14
Middle	7	2.7	3.4
Bottom	10	1	1

When KCl crystals were quenched, the concentration of monomer increased and those due to the trimer and trimer interaction decreased with the trimer interaction showing the greatest decrease. As in the case of the dilute samples the interaction bands were very weak and negligible compared to those of the monomer and trimer. Two weak bands which had not previously been observed in these crystals were observed and will be discussed later. As expected, annealing the KCl crystals gave results opposite to those observed in the quenching experiments. Relative concentrations of the monomer, trimer, and trimer interaction as determined from the intensities of corresponding modes were then known after three different thermal treatments. Information on the absorption coefficients of the monomer and trimer is available from these data if the absorption coefficient of the interaction bands are the same as those of the unperturbed trimer bands. The amount of trimer present is then related to the

sum of the trimer band and the trimer interaction bands. The total

amount of boron or number of BO_2 groups present is

$$C = 3C_T + C_M \qquad (3\text{-}4)$$

where C_T and C_M are the concentrations of the trimer and mon-

omer respectively. Using Beer's law, Equation 3-4 becomes

$$\frac{A_M}{t} = -3\frac{a_M}{a_T}\frac{A_T}{t} + \frac{1}{2.3}Ca_M \qquad (3\text{-}5)$$

in which A, a, and t refer to absorbance, absorption coeffi-

cient, and the thickness of the sample respectively. From a plot of

A_M/t versus A_T/t, a_M and a_T may be determined from the

slope and A_M/t intercept. Although it might be simpler to plot

A_M versus A_T, the thickness has been included because the sam-

ples were repolished after annealing which resulted in a thickness at-

tenuated by $< 10\%$. This raises the question of error due to possible

inhomogeneity. Since the amount of boron was shown to vary $< 10\%$

both perpendicular to the growth axis and for a distance of one cm

parallel to the axis, the error due to inhomogeneity is known to be

small. Such plots which are reproduced in Figure 15 for two crystals

doped with enriched ^{10}B and ^{11}B gave values for a_M which were

different by 30% while those for $a_T(\omega_7)$ were within 1% of each other.
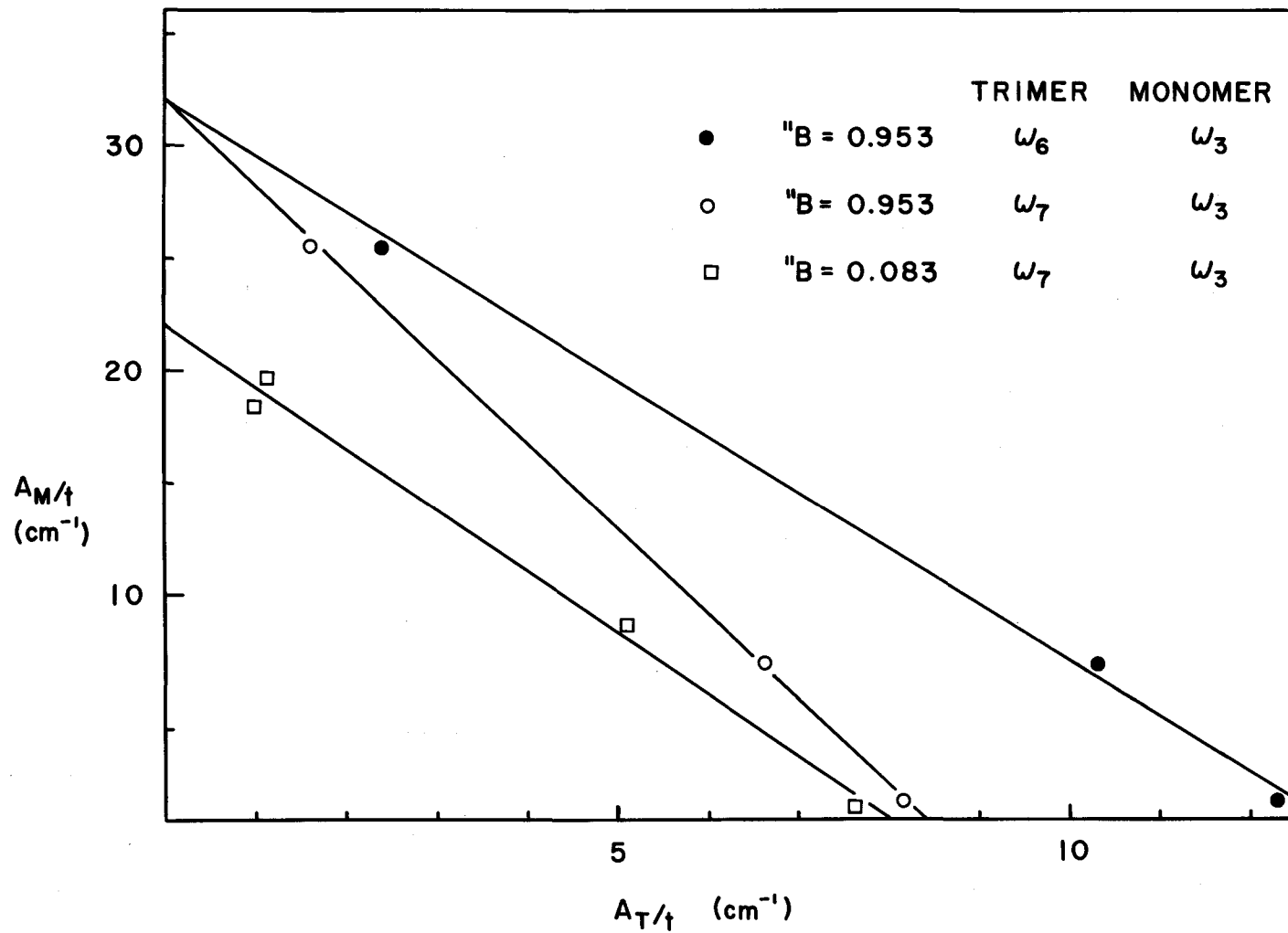
Figure 15. A_M/t at $T \simeq 300°$ K versus A_T/t at $T \simeq 100°$ K in KCl crystals at various thermal histories.

The assumption that the absorption coefficients of the trimer and the interaction bands are equal may not be valid; or, more likely, significant overlapping may result between these bands including smaller interaction bands which have not been considered, thereby causing the observed uncertainty. However, the observed linearity of these plots is good evidence that the species which has been attributed to the trimer is composed of BO_2^- units; although no information is available from these plots on the number of BO_2^- units. Average values are listed in Table 17 as well as the value of a_M found in KBr.

Table 17. Absorption coefficients.

		KCl $(cm^{-1}ppm^{-1})*$	KBr $(cm^{-1}ppm^{-1})*$
a_M	ω_3	.9	.71
a_T	ω_6	1.2	
a_T	ω_7	.8	

* In molar fraction

The more dilute samples of KBr were found to contain nearly all monomer and only very small amounts of trimer in solid solution and in a second phase, thereby allowing the absorption coefficient of the monomer to be determined. A quenching experiment on a more concentrated KBr sample, as shown in Figure 2, resulted in the complete removal of the precipitated trimer, the reduction of the trimer bands to very weak bands, and a very large increase in metaborate

monomer producing the largest concentration of monomer observed in this laboratory. One very weak and two weak bands were observed in the quenched KBr crystal which may be related to the bands in KCl produced upon quenching. In KBr these bands may have been obscured by the broad second phase bands before quenching. Neglecting these for the moment, this result demonstrates that the broad and sharp features which have been assigned to the trimer in a second phase and in solid solution are due to impurities which contain BO_2^- units. If the trimer is made of BO_2^- groups, we may conclude that the trimer interaction bands in KCl which are nearly removed by quenching are also due to an impurity which may be constructed with BO_2^- groups.

The metaborate monomer was found to be more soluble as the size of the lattice was increased from NaCl to KBr, as is expected for a monovalent ion which fits substitutionally in the lattice. This trend was not observed for the trimer consistent with the argument that the solubility is greater when the fixed distances between the three negative charges on the trimer more closely approach the anion-anion distance in the lattice. From the above results we also know that an equilibrium exists between the monomer and the trimer which may be in solid solution, near another trimer ion, or in a precipitate. This equilibrium favors a larger concentration of monomer as the temperature is increased. The monomer ions being small diffuse through the crystal in a random manner, but the larger trimer ions are not

expected to move as a unit. If the temperature of the crystal is lowered rapidly, the monomer ions lose their ability to move. Because the equilibrium between the monomer and trimer depends upon the probability of having three monomer ions at approximately the same position in the lattice, the concentrations of the various impurities correspond to the equilibrium which existed at the temperature from which the crystal was quenched. When the temperature is lowered slowly the equilibrium would then roughly correspond to the temperature range at which the monomer becomes nearly immobile.

After quenching KCl and KBr crystals, several sharp and weak bands were found which were not observed before. These bands became significantly larger in KCl as the starting temperature of the quench was increased, whereas all the nearby bands became slightly less intense as shown in Figure 4. This behavior suggests that either another impurity is being formed which is favored by higher temperatures or the trimer ion is at a different position in the lattice. These bands are more intense in KBr even though the KBr crystal was quenched from a temperature less than or equal to those used with KCl. The frequencies and intensities in KCl seem to fit a pattern very similar to the one shown in Figure 8 for the trimer of metaborate except all six components are resolved. Furthermore, the frequencies are somewhere between those observed for the trimer ion in solid solution and in a second phase. Therefore, these bands are

very tentatively assigned to metaborate trimer ions in some unknown
position.

Table 18.   Bands observed upon quenching. $T \cong 100°\,K.$

KBr	KCl			
^{11}B	$3\,^{11}B$	$2\,^{11}B+\,^{10}B$	$^{11}B+2\,^{10}B$	$3\,^{10}B$
1398.8	1402.3			1459
1196.5	1202.2	1204.3	1215.6	1246.4
		1234.2	1244.8	
753				

IV. NORMAL COORDINATE ANALYSIS OF THE TRIMER
OF METABORATE

Symmetry Considerations and Internal Symmetry
Coordinates

The trimer of metaborate has a total of nine atoms and there-
fore $3N - 6 = 21$ vibrational degrees of freedom which consist of

$2N - 3 = 15$ in-plane and $N - 3 = 6$ out-of-plane, vibrational de-

grees of freedom. When all three boron atoms are isotopically equiv-

alent the trimer belongs to the D_{3h} group, whereas the replacement

of one boron atom with an isotopically nonequivalent one lowers the

symmetry to C_{2v}. The irreducible representations are

$$\Gamma = 3A_1' + 2A_2' + 5E' + 2A_2'' + 2E'' \qquad (4-1)$$

and

$$\Gamma = 8A_1 + 2A_2 + 4B_1 + 7B_2 \qquad (4-2)$$

for D_{3h} and C_{2v} respectively. The C_{3v} symmetry of the proposed

site would lower the symmetry to C_{3v} and C_s for the trimer belonging

to the D_{3h} and C_{2v} groups respectively. Correlation diagrams be-

tween these groups corresponding to both isotopic and site symmetry

perturbations and the activity of the various modes are shown in Fig-

ure 16.

In this analysis the trimer was treated as if it consisted of
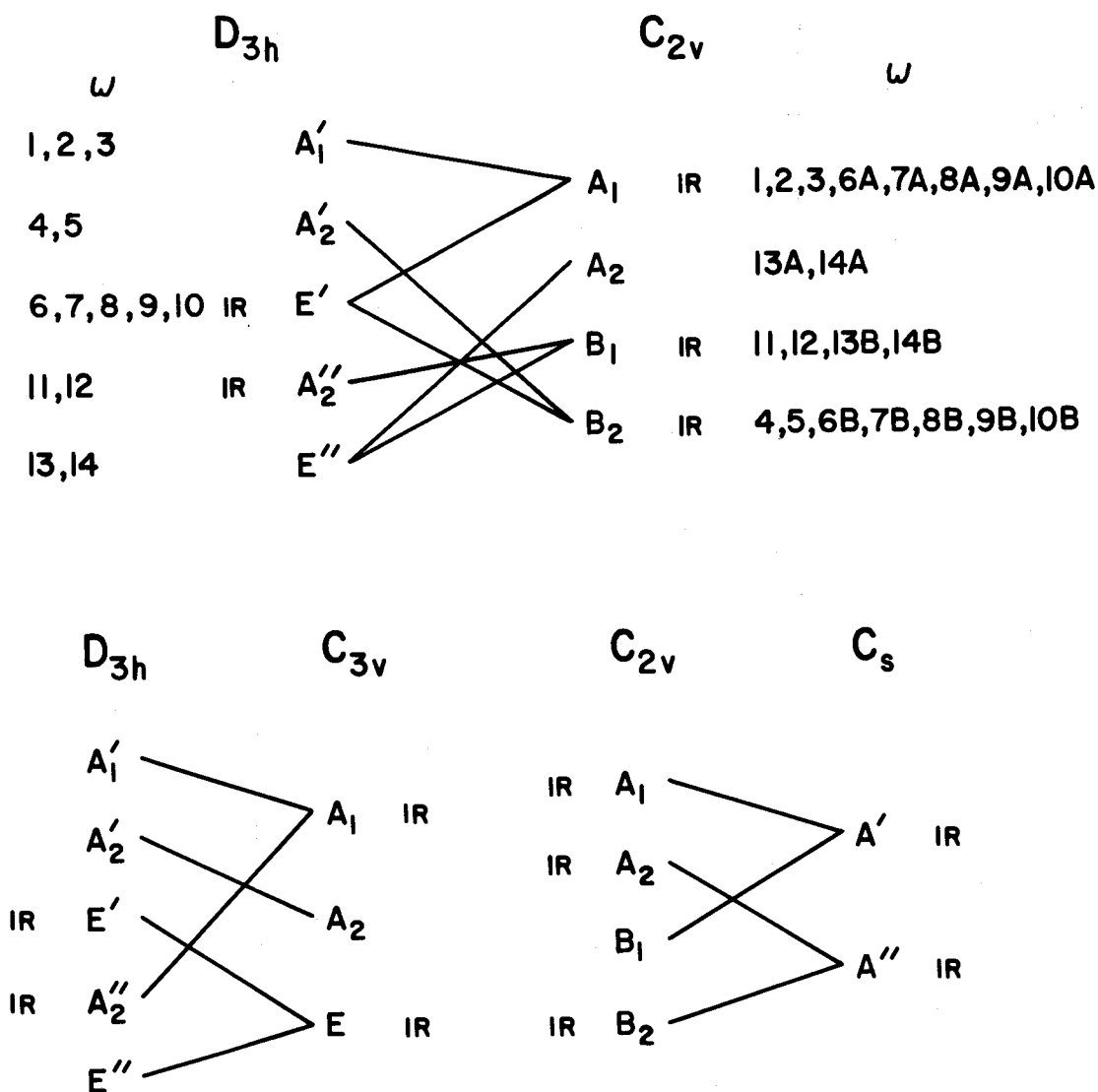
Figure 16. Correlation diagrams and spectral activity corresponding to isotopic and site symmetry perturbations of the metaborate trimer in alkali halides with the NaCl structure.

three symmetrically equivalent BO_3 groups which were loosely coupled together. For convenience each internal symmetry coordinate was constructed from symmetrically complete sets of equivalent internal coordinates; r_i, s_j, β_i, a_j, z_i, and Z_i which are described and depicted in Figure 17. The irreducible representations for these sets are listed in Table 19, and the internal symmetry coordinates formed from these internal coordinates are given in Appendix I. The second set of E' and E'' symmetry coordinates are not necessary and have been included merely for completeness.

Table 19. Irreducible representations of $(BO_2^-)_3$ for D_{3h} symmetry.

$\Gamma^{(\gamma)}$	$\eta^{(\gamma)}_{total}$	$\eta^{(\gamma)}_{vib.}$	$\eta^{(\gamma)}_r$	$\eta^{(\gamma)}_s$	$\eta^{(\gamma)}_a$	$\eta^{(\gamma)}_\beta$	$\eta^{(\gamma)}_z$	$\eta^{(\gamma)}_Z$
A_1'	3	3	1	1	0	1	0	0
A_2'	3	2	0	1	1	0	0	0
E'	6	5	1	2	1	1	0	0
A_1''	0	0	0	0	0	0	0	0
A_2''	3	2	0	0	0	0	1	1
E''	3	2	0	0	0	0	1	1

G and F Matrices

The elements of both matrices were obtained by hand calculation, first for the internal coordinates and then for the internal symmetry coordinates. The F matrices corresponding to the D_{3h} internal

r_i = change in exterior B-O^- bond length

s_j = change in interior OB-O bond length

a_j = change in exterior O-B-O^- angle

β_i = change in interior O-B-O angle

γ = equilibrium interior B-O-B angle

z_i = $r*\sin\theta$

Z_i = $-s\cos\gamma\sin\phi$

θ = angle formed by external O^- and plane of BO_2

ϕ = angle formed by interior ring oxygen and plane of the remainder of ring.

Where + and - numbers denote relative out-of-plane motion of the atoms.

* No subscript denotes equilibrium value of coordinates

Figure 17.   Internal coordinates of the metaborate trimer.
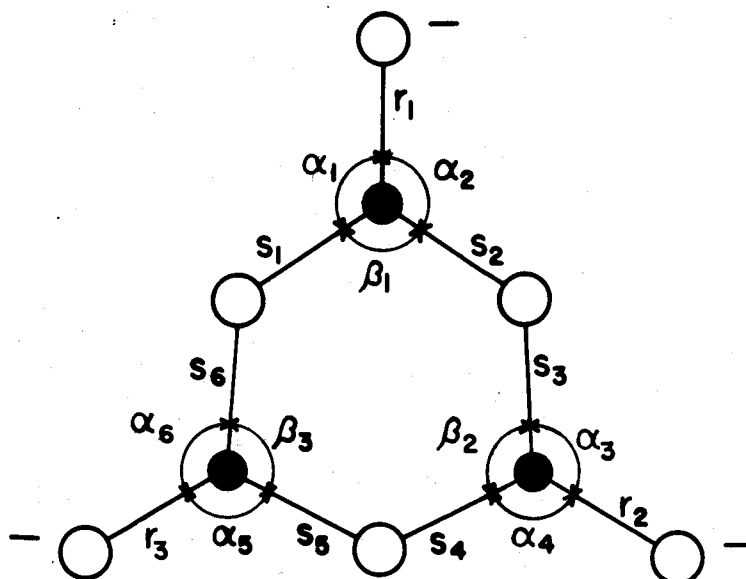
IN – PLANE
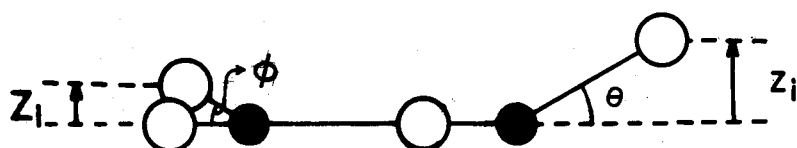
SIDE   VIEW
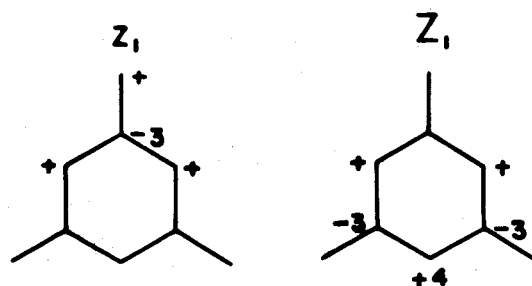
TOP   VIEW

OUT – OF – PLANE

coordinates and internal symmetry coordinates are given in Table 20

and Appendix II. Because of their complexity the corresponding G

matrices, which are similar in form, are not shown. Although the

formation of the G matrix was normally straightforward, the equili-

brium bond lengths and angles were assumed to be equal to those for

the trimer in $K_3(BO_2)_3$ published by Zachariasen (45) and given in Ta-

ble 21. A comparison with the corresponding values in $Na_3(BO_2)_3$

published by Mazerio et al. (30) reveals the order of magnitude of the

uncertainty that may be involved in this assumption. Their values of

1.280 and 1.433 $\overset{\circ}{A}$ are the smallest and largest ever observed for the

triangular boron-oxygen bond.

In this normal coordinate analysis a generalized valence force

field has been employed whose force constants have been tabulated in

the F matrix in Table 20. All the terms corresponding to a potential

interaction between two internal coordinates which are in different

BO_3 groups, with the exception of ϕ_z', have not been included due

to the complexity of the potential function. The force constants

$$\phi_r = 6.96 \quad \text{and} \quad \phi_s = 5.57 \text{ md}/\overset{\circ}{A} \tag{4-3}$$

corresponding to a change in the exterior B-O⁻ and interior OB-O

bond lengths were calculated using the empirical function

$$\phi_{\bar{r}} = 38.5 \, \bar{r}^{-6} \tag{4-4}$$

Table 20. F matrix for internal coordinates of metaborate trimer.

F	r_1	r_2	r_3	s_1	s_2	s_3	s_4	s_5	s_6	β_1	β_2	β_3	α_1	α_2	α_3	α_4	α_5	α_6
r_1	ϕ_r	0	0	ϕ'_s	ϕ'_s	0	0	0	0	$s\phi_{r\beta}$	0	0	$\sqrt{rs}\,\phi'_{r\beta}$	$\sqrt{rs}\,\phi'_{r\beta}$	0	0	0	0
s_1				ϕ_s	ϕ'_s	0	0	0	0	$s\phi'_{r\beta}$	0	0	$\sqrt{rs}\,\phi'_{r\beta}$	$\sqrt{rs}\,\phi_{r\beta}$	0	0	0	0
β_1										$s^2\phi_\beta$	0	0	$s^2\phi'_\beta$	$s^2\phi'_\beta$	0	0	0	0
α_1													$rs\phi_\beta$	$s^2\phi'_\beta$	0	0	0	0

F	z_1	z_2	z_3	Z_1	Z_2	Z_3
z_1	$s^2\phi_z$	$s^2\phi'_z$	$s^2\phi'_z$	$s^2\phi_{zZ}$	$s^2\phi'_{zZ}$	$s^2\phi'_{zZ}$
Z_1				$s^2\phi_Z$	$s^2\phi'_Z$	$s^2\phi'_Z$

according to Decius (8, 9) where $\bar{r}$ is the equilibrium bond length.

Consequently the uncertainty in r and s mentioned in the previous paragraph will produce a relative uncertainty in $\phi_{\bar{r}}$ which is six times larger. The effect of this and other uncertainties upon the predicted eigenvalues will be discussed later in this chapter. There is no information available on the restoring forces which are due to an interaction between internal coordinates in adjacent BO_3 groups. Because these forces are thought to be small, the corresponding force constants have been set equal to zero. Values for the remaining, in-plane force constants or combinations of them, ϕ'_s (.98 md/$\overset{\circ}{A}$), $\phi_\beta - \phi'_\beta$, and $\phi_{r\beta} - \phi'_{r\beta}$, which are thought to be similar to those for the borate ion, were borrowed from the values observed by Steele and Decius (39). Unfortunately individual values of ϕ_β, $\phi_{r\beta}$, and $\phi'_{r\beta}$ were needed; therefore, several reasonable values have been tried.

Table 21. Bond lengths and angles in the metaborate trimer.

	$K_3(BO_2)_3$	$Na_3(BO_2)_3$
$r(B-O^-)$	1.33 $\overset{\circ}{A}$	1.280 ± .016 $\overset{\circ}{A}$
$s(BO-B)$	1.38 $\overset{\circ}{A}$	1.433 ± .009 $\overset{\circ}{A}$
$\angle$ O-B-O	113.5°	

The situation for the out-of-plane blocks of the F matrix is less favorable. There are six force constants only one of which is similar

to the out-of-plane force constant for the borate ion, and there is no available information on the remaining five. Therefore, using the experimental frequencies which have been assigned to the corresponding modes in the present investigation and in that of Hisatsune and Suarez (28), the force constants were obtained by solving the secular equation simultaneously for ^{10}B and ^{11}B. The average of the values for the out-of-plane force constant obtained by Steele and Decius (39), 1.815 md$\overset{\circ}{A}$ ($s^2 .953$ md/$\overset{\circ}{A}$), agrees well with the calculated value of 1.855 md$\overset{\circ}{A}$ given in Table 22. The small value of ϕ_z', the interaction force constant between two z coordinates in adjacent BO_3 groups, is consistent with the assumption that the trimer ion may be described as three BO_3 groups which are loosely coupled together. There are two values for each force constant because of the quadratic nature of the problem. There are actually four sets of values, but two of these sets lead to answers which are physically unrealistic.

Table 22. Calculated out-of-plane force constants for the metaborate trimer.

	md·$\overset{\circ}{A}$	
	1	2
ϕ_z	1.855	1.416
ϕ_z'	.003	.222
ϕ_{zZ}	.594	.390
ϕ_{zZ}'	-.691	-.589
ϕ_Z	.763	.723
ϕ_Z'	-.178	-.157

Normal Coordinates and Eigenvalues

The normal coordinates (column matrix Q) are related to the internal symmetry coordinates (column matrix S) by the linear transformation

$$S = LQ \qquad (4\text{-}5)$$

or upon multiplying on the left by L^{-1}

$$Q = L^{-1}S \qquad (4\text{-}6)$$

Substitution of (4-6) into the kinetic and potential energies of vibration results in the well known secular equation in matrix notation

$$(GF - \Lambda)L = 0 \qquad (4\text{-}7)$$

as shown in Wilson, Decius, and Cross (43).

In order to solve the secular equation, an unsymmetric eigenvalue program obtained from the University of Wisconsin and adapted to a CDC-3300 computer was used in conjunction with matrix multiplication and matrix inversion subroutines. Furthermore, the elements G_{ij} for C_{2v} symmetry were numerically evaluated with the aid of the computer. Solutions of the secular equation for D_{3h} symmetry, which are given in Appendix III, depend strongly on the assumed values of ϕ_β, $\phi_{r\beta}$, and $\phi'_{r\beta}$. Also when some of the B-O stretching

force constants were altered corresponding to a five percent change in the equilibrium B-O distances, changes of up to 10% in the eigenvalues (15% for ω_4) were observed.

It is evident that this calculation can be used only as a rough prediction of the experimental frequencies and normal coordinates to aid in the assignment and not as a means to refine the force constants. A comparison between one set of predicted frequencies which is in good agreement with the best understood fundamentals and the complete assignment of the observed fundamentals in KCl is made in Table 23. ω_1 and ω_4, which are infrared inactive for D_{3h} symmetry and weakly active for C_{2v} symmetry, are predicted to be near ω_6, and between ω_6 and ω_7 respectively. Furthermore, several possible E' combinations involving an A_1' or A_2' mode occur near ω_6, but only one such combination occurs near ω_7, consistent with the relatively complex and simple patterns observed near ω_6 and ω_7.

Solution of the secular equation for C_{2v} symmetry predicts that the eigenvalues for the trimer containing equivalent boron isotopes bracket the eigenvalues of the mixed isotope trimer as is experimentally observed. In addition, the solution for C_{2v} symmetry yields information on the splitting of modes previously degenerate under D_{3h} symmetry, which is depicted in Table 24.

The linear transformation L^{-1} corresponding to the set of eigenvalues given in Table 23, which are in reasonable agreement with the

experimental values observed for the trimer of metaborate and simi-
lar compounds, is given in Appendix IV. This allows the normal
modes to be described in terms of the internal coordinates and in
terms of vibrations of individual atoms. However this description
must not be pushed too far.

Table 23. Predicted and experimental, in-plane fundamentals of the
metaborate trimer.

	Predicted eigenvalues for D_{3h} symmetry when $\phi_\beta = .80$, $\phi_{r\beta} = -.50$, and $\phi'_{r\beta} = .25$ md/$\mathring{A}$ (cm^{-1})		Experimental fundamentals in KCl at $T \simeq 100°$ K (cm^{-1})	
	^{11}B	^{10}B	^{11}B	^{10}B
ω_1	1315	1360	1435*	1484*
ω_2	801	801		
ω_3	548	555	588	604
ω_4	1224	1255	1258	1279
ω_5	756	768		757
ω_6	1367	1411	1430.6	1481.4
ω_7	1147	1177	1175.2	1208.8
ω_8	1012	1025	936.8	938.9
ω_9	427	430	466	472
ω_{10}	372	373	290	295

* Values for the trimer containing 2^{11}B+^{10}B and ^{11}B+2^{10}B.

Table 24. Predicted isotopic splitting of degenerate modes of the metaborate trimer.

	ω_6, ω_9 and ω_{10}			ω_7 and ω_8			ω_{13} and ω_{14}		
$3\,^{10}B$	E'			E'			E''		
$2\,^{10}B + {}^{11}B$	B_2		A_1	A_1		B_2	A_2		B_1
$^{10}B + 2\,^{11}B$		A_1	B_2		B_2	A_1		B_1	A_2
$3\,^{11}B$			E'			E'			E''

V. ASSIGNMENTS FOR THE METABORATE TRIMER

Because the experimental spectra are very complex, the follow-ing assignments, even though they fit the experimental facts, may not necessarily be entirely correct. This complexity is due in part to the presence of at least four species which are BO_2^-, $(BO_2^-)_3$, $K_3(BO_2)_3$ or $Na_3(BO_2)_3$, and possibly $[(BO_2^-)_3]_n$. In addition, the trimer ion which is normally the primary constituent has 14 fundamental vibra-tions on the basis of D_{3h} symmetry. Seven are infrared active with five of them being doubly degenerate. When the symmetry is lowered to C_{2v} by an isotopic perturbation or to C_{3v} and C_s by the site sym-metry, degeneracies are removed and/or some of the inactive funda-mentals become weakly active. This is shown in the correlation dia-grams in Figure 16. There are also many possible combinations which, if they belong to the proper symmetry species, may be in Fermi resonance with the fundamentals.

The vibrational modes have been classified according to the type of motion involved, where possible, to aid in the discussion. This classification consists of in-plane, stretching and bending modes $(A_1^{'}$, $A_2^{'}$, and $E^{'})$, and out-of-plane, bending modes $(A_2^{''}$ and $E^{''})$.

In-Plane Modes

The assignments of the in-plane and out-of-plane modes in KCl, NaCl, and KBr are presented in Table 25. The assignments in NaCl and KBr are less complete because of the presence of very broad

Table 25. Assignment of fundamental modes of $(BO_2^-)_3$ in NaCl, KCl, and KBr. (cm^{-1}) $T \cong 100°K$

D_{3h}	C_{2v}		NaCl $3^{11}B$	NaCl $2^{11}B+^{10}B$	NaCl $^{11}B+2^{10}B$	NaCl $3^{10}B$	KCl $3^{11}B$	KCl $2^{11}B+^{10}B$	KCl $^{11}B+2^{10}B$	KCl $3^{10}B$	KBr $3^{11}B$	KBr $2^{11}B+^{10}B$	KBr $^{11}B+2^{10}B$	KBr $3^{10}B$
A_1'	A_1	ω_1		1476.6				1434.7	1483.5					
	IR	ω_2												
		ω_3	611			631	588			604				
A_2'	B_2	ω_4	1290				1258			1279				
	IR	ω_5				777		732	752.5	757				747
E' IR	A_1+B_2 IR	ω_6	1467.8	1468 B_2 / 1502.7 A_1	1503 A_1 / 1527.3 B_2	1529.3	1430.6	1430.8 B_2 / 1460.8 A_1	1459.4 A_1 / 1480.8 B_2	1481.4	1419.4			1466.8
		ω_7	1209.5	1210 A_1 / 1234.2 B_2	1223.2 B_2 / 1243 A_1	1243.6	1175.2	1175.9 A_1 / 1198.7 B_2	1188.3 B_2 / 1207.9 A_1	1208.8	1166.5	1166.5 A_1 / B_2	1179.1 B_2 / 1199.A_1	1199.3
		ω_8	955			959	936.8			938.9	936			936
		ω_9	481				466			472	466			472
		ω_{10}	300				290			295	290			295
A_2'' IR	B_1 IR	ω_{11}					773.5	781.1	786.6	791.1	765			785
		ω_{12}												
E''	A_2+B_1	ω_{13}	739.6				720.5	A_2 / 720.5 B_1	720.9 B_1 / A_2	724.1	715.6			718.4
	B_1;IR	ω_{14}												

81

bands which have been assigned to a second phase of the appropriate salts of the trimer ion. Although the assignment of ω_6 and ω_7 to the strong lines in the stretching region of the spectrum was straight forward, the assignment of individual lines to isotopic components was somewhat more difficult. Under C_{2v} symmetry E' is split into A_1 and B_2 resulting in six possible components. Using the splitting predicted by the normal coordinate analysis given in Table 24, the experimental components and their intensities may be explained with the proposed patterns shown schematically for ω_6 and ω_7 in Figure 8. The experimental pattern for ω_7 is close to the theoretical one except for minor discrepancies in the intensities. These discrepancies are caused by two shoulders at about 1190 and 1200 cm^{-1}, which are due to trimer interaction, and by less overlapping between E' and A_1 at the high frequency component compared to the low frequency component.

The theoretical pattern for ω_6 is, however, not sufficient to explain the experimental lines in this region. Rather than the expected singlet which is observed in ^{10}B enriched crystals, a doublet is present in spectra of ^{11}B enriched crystals. The singlet in ^{10}B enriched crystals is about 50% larger than the corresponding component of ω_7. Although both members of the doublet are much less intense than the corresponding component of ω_7, the sum of the absorbances of the two members of the doublet is about 50% larger than the corresponding component of ω_7 as in the enriched ^{10}B case. In KCl and perhaps NaCl and KBr crystals containing enriched ^{11}B, the two members of the doublet are of nearly equal intensity; however, they seemingly are

not equal in some crystals containing mixtures of boron isotopes. The

additional intensity of the lower frequency member in these cases is

due to a shoulder which has also caused this band to be shifted to a

higher frequency by one wavenumber. This shoulder and many other

bands in this region are due to interactions between trimer ions.

The presence of this doublet and its anamalous intensities may

be explained by Fermi resonance between ω_6 and $2\omega_{13}$. Since the fre-

quency of ω_{13} depends very weakly upon the boron isotope, ^{11}B rich

components of $2\omega_{13}$ and ω_6 are much closer than those of ^{10}B result-

ing in a stronger Fermi resonance.

The constant b which is related to the perturbation or repulsion

of the two energy levels has been calculated for some of the isotopic

components by means of Equation 5-1.

$$\begin{vmatrix} \omega_1^0 - \omega & b/\sqrt{2} \\ b/\sqrt{2} & \omega_2^0 - \omega \end{vmatrix} = 0 \qquad (5\text{-}1)$$

Because of the nearly equal intensities of the two members of the

doublet in KCl and NaCl, the unperturbed energy levels are assumed

to be midway between the experimental lines. The same anharmonic-

ities were used in NaCl, KCl, and KBr and have been listed in Table

26 as have the other details of this calculation. This is only an ap-

proximate calculation because there are several weak bands nearby

assigned to E' combinations whose presence have been neglected. The

combination and overtone bands are listed in Table 27, and arguments

for their assignments are given in the next paragraph. Because

$\omega_7 + \omega_{10}$ is closer than $2\omega_{13}$ to the fundamental ω_6 for the $3^{10}B$ trimer, the approximation is not a good one for $3^{10}B$. A better approximation would be to consider Fermi resonance between ω_6, $2\omega_{13}$, and $\omega_7 + \omega_{10}$; however, this would involve solving a 3 x 3 determinant with six unknowns, and if the assignments of the combinations are correct, then the determinant is even larger.

Table 26. Fermi resonance calculation. (cm^{-1})

	KCl			KBr		NaCl
	$3^{11}B$ E'	$2^{11}B+^{10}B$ B_2	$3^{10}B$ E'	$3^{11}B$ E'	$3^{10}B$ E'	$3^{11}B$ E'
$2\omega_{13}$	1444.0	1444.6	1441.0	1434	1429.3	1483.3
$2\omega_{13}^0$	1437.3	1438.3	1443.0	1427.6	1431.6	1475.6
ω_6^0	1437.3	1437.3	1479.5	1425.8	1464.5	1475.5
ω_6	1430.6	1431.0	1481.5	1419.4	1466.5	1467.8
Anharmonicity	3.7	4.4	5.2	3.7	5.2	3.7
b	9.5	9.6	12.4	10.2	12.6	11.0
$\omega_{13}*$				715.6	718.4	739.6

* Calculated from $2(\omega_{13}) - 2\omega_{13}^0$ = Anharmonicity.

There are many weak bands which occur near the E' fundamentals ω_6, ω_7, and ω_8 and which may be assigned to combination modes consistent with the trimer model. In general, the further removed a nearby band is from the fundamental ω_6, the less intense it is. There is only one band near ω_7 and one near ω_8, and their relative intensities

Table 27. Overtones and combinations of $(BO_2^-)_3$ in NaCl, KCl, and KBr. (cm^{-1}) $T \simeq 100°$ K

	NaCl		KCl		KBr	
	^{11}B	^{10}B	^{11}B	^{10}B	^{11}B	^{10}B
$2\omega_9$	962 w, b		931 w, b	943 w, b		944 w, b
$\omega_5+\omega_9$		1264 m, b		1229. 2 m		1218. 8 m
$\omega_8+\omega_9$	1436. 5$^+$		1401	1410	1402$^+$	
$2\omega_{13}$	1483. 3 s		1444. 0 s	1441. 0 m	1434$^+$	1429. 3 m
$\omega_7+\omega_{10}$	1509 sh		1465. 4 m	1503. 7 m	1456. 0$^+$	1494. 8$^+$
$\omega_{11}+\omega_{13}$			1497. 7 vw	1519. 5 vw		
$\omega_3+\omega_8$	1565. 6 w	1589. 8 vw	1524. 8 w	1542. 5 w		
$\omega_4+\omega_{10}$	1590 vw		1547. 5 vw	1574. 0 vw		
$\omega_{10};{}^*(\omega_7+\omega_{10})-\omega_7$	300		290	295	289	295
$\omega_9; 1/2(2\omega_9)$	481		466	472		472
$\omega_9; (\omega_8+\omega_9)-\omega_8$	481. 5		464		466	
$\omega_3; (\omega_3+\omega_8)-\omega_8$	611	631	588	604		
$\omega_5; (\omega_5+\omega_9)-\omega_9$		777		757		747
$\omega_4; (\omega_4+\omega_{10})-\omega_{10}$	1290		1258	1279		

* Neglecting anharmonicity and Fermi resonance.

$^+$ Partially obscured by broad bands assigned to the trimer in a second phase.

are consistent with those near ω_6. From this it is reasoned that these weak bands are combination bands which belong to the E' symmetry species and have consequently obtained some of their intensity from the fundamental through Fermi resonance. The forbidden and the weak, allowed fundamentals obtained from these combination bands, given in Table 27, were found to be comparable with infrared and Raman data from $Na_3B_3O_6$ and related compounds.

A weak doublet near 950 cm^{-1} has been assigned to ω_8 and $2\omega_9$. The stronger line which has been assigned to ω_8 does not vary appreciably with a change in boron isotope and must, therefore, be due primarily to a movement of the oxygen atoms. It is worthwhile noting that the normal coordinate analysis for D_{3h} symmetry predicts a degenerate mode near 1000 cm^{-1} due primarily to a movement of the oxygen atoms. Although the fundamental ω_9 was not observed in KCl or NaCl because of the strong lattice absorption, a very weak and very broad band was observed in KBr at about 470 cm^{-1} at room temperature. This assignment of ω_8 and ω_9 agrees with the assignment of Hisatsune and Suarez (28) for the trimer ion and with those of similar molecules which contain the $(BO_2^-)_3$ ring (29 and 33). Hisatsune and Suarez also report that ω_9 is a very weak fundamental.

The remaining E' mode, ω_{10}, was obtained indirectly from the combination $\omega_7 + \omega_{10}$. In KBr weak bands were observed at room temperature at 303 and 304.5 cm^{-1} for enriched ^{11}B and ^{10}B

respectively. These may be ω_{10} but this would require an anharmonicity of at least 10 cm^{-1}; the temperature effect is in the opposite direction.

All but two of the five forbidden fundamentals belonging to the A_1' and A_2' symmetry species were obtained from combination bands in KCl. These assignments were made with the aid of Raman data for similar compounds (25, 33) which are reproduced in Table 28 for the Raman active A_1' modes.

Table 28. A_1' modes of $B_3O_3X_3$ observed in Raman spectra by Goubeau and Keller (25), and Parsons (33). (cm^{-1})

	ω_1	ω_2	ω_3
$B_3O_3Cl_3$	1037	807	333
$B_3O_3[N(CH_3)_2]_3$	1147	804	537
$B_3O_3(CH_3)_3$	1155	807	539
$B_3O_3(OCH_3)_3$	1286	804	556
		849*	
$B_3O_3(OH)_3$		819	598

* Unassigned by authors

Latimer and Devlin (29) observed two weak and broad lines at 826 and 896 cm^{-1} for ^{11}B, and at 838 and 903 cm^{-1} for ^{10}B in the infrared spectra of thin films of $(BOF)_3$. They suggest that 826 and 838 are ω_2 which has been activated by the lattice. If their activation argument is valid, then 896 and 903 cm^{-1} might also be ω_2.

The predicted normal coordinate corresponding to ω_2 involves a motion of the ring oxygen atoms, while the boron atoms and exterior oxygen ions do not move appreciably. Just the opposite is true for ω_1, whereas the expected motion of the exterior oxygen ions in ω_3 is about two or three times greater than that of the oxygen and boron atoms in the ring. In light of this, if the mass of the oxygen ion is increased either by substitution of an isotope or an isoelectronic atom such as fluorine, a progressively larger decrease in the frequencies of ω_2, ω_3, and ω_1 is expected with ω_1 showing the greatest decrease. This pattern is consistent with the frequencies reproduced in Table 28. Although, without Raman data on ω_1 and ω_3 of $(BOF)_3$, less can be said about the frequencies of these A_1' modes; it has been assumed, subject to further information, that ω_2 and ω_3 are approximately equal to 820 and 600 cm^{-1} and that ω_1 is somewhat larger than 1290 cm^{-1}. Therefore, 588 and 604 cm^{-1} in KCl, and 611 and 631 cm^{-1} in NaCl have been assigned to ω_3; whereas 777, 757, and 747 cm^{-1} were assigned to ω_5 ($3^{10}B$) in NaCl, KCl, and KBr. None of the observed combination bands were thought to contain ω_2 because a very weak Fermi resonance was expected due to large differences in frequency between the fundamentals and possible combinations if $\omega_2 \simeq 820$ cm^{-1}. ω_4 rather than ω_1 has been assigned to 1258 and 1279 cm^{-1} in KCl primarily on the basis or arguments in the next paragraph as well as the frequency argument above.

Two strong lines at 1434.7 and 1483.5 cm^{-1} having the proper

change in intensity with change in boron isotope have been assigned to

the $2^{11}B + {}^{10}B$ and $^{11}B + 2^{10}B$ components of ω_1. When an isotopic

perturbation lowers the symmetry from D_{3h} to C_{2v}, the A_1' and A_2'

modes become A_1 and B_2 modes which are expected to be, at most,

weakly active. However if these modes are near any of the fundamen-

tals of the same symmetry species, an interaction should occur.

These two lines are very near the B_2 components of ω_6 and $2\omega_{13}$ with-

out apparently disrupting the expected pattern. In contrast, both of

these lines are symmetrically separated by about 25 cm^{-1} from the

A_1 components of ω_6. Therefore these lines are thought to belong to

the A_1 symmetry species and have been assigned to ω_1. If the fre-

quency differences between all four components of ω_1 are assumed to

be the same, $\Pi \dfrac{\omega_i'}{\omega_i}$ is larger than predicted by the product rule. How-

ever if an interaction occurs between the A_1 components of ω_6 and ω_1

when the symmetry is reduced to C_{2v}; there is no theoretical reason

to believe an equal spacing between components should exist.

The product rule has been applied to various symmetry species

where the assignments are complete, and the results are given in Ta-

ble 29. ω_6^0 has been employed in this calculation, whereas experimen-

tal values for the other frequencies neglecting anharmonicities and

Fermi resonance have been used. In the latter frequencies the Fermi

resonance is much weaker, and no information is easily attainable

concerning the magnitude of this resonance.

Table 29. Teller-Redlich product rule for $(BO_2^-)_3$ with D_{3h} symmetry in KCl and KBr.

Symmetry species	Host	$\Pi \dfrac{\omega_k'}{\omega_k}$		
A_1'			$\Pi(\frac{m}{m'})^{1/2}$	$= 1.049$
A_2'			$\Pi(\frac{m}{m'})^{1/2}(\frac{I_Z}{I_Z'})^{1/2}$	$= 1.043$
E'	KCl	1.093	$\Pi(\frac{m}{m'})(\frac{M'}{M})$	$= 1.087$
	KBr	1.088		
A_2''			$\Pi(\frac{m}{m'})^{1/2}(\frac{M'}{M})^{1/2}$	$= 1.036$

where m = mass of atoms
M = mass of molecules

Out-of-Plane Modes

According to the arguments and dimensions given in Chapter III, the trimer in solid solution should be distorted. Since this distortion is due to three potassium ions lying above the plane of the ring and one lying below this plane, any motion perpendicular to the plane of the ring should be much more restricted than a motion in the plane. As there is much more space available to the trimer in a crystal of $K_3(BO_2)_3$, it is logical that the restoring force for an out-of-plane motion should be larger and the amplitude smaller for the trimer in

an alkali halide compared to $K_3(BO_2)_3$.

Four medium intensity bands between 781 and 791 cm^{-1} in KCl have been assigned to ω_{11}, one of the two allowed A_2'' fundamentals. As expected, these frequencies are larger than those observed by Büchler and Marram (5), Goubeau and Hummel (24), and Hisatsune and Suarez (28); and the relative intensities of these bands are less than the corresponding bands observed by Hisatsune and Suarez. Furthermore, the bands at 387 and 388 cm^{-1} in a KBr pellet that they describe as medium intensity bands and assign to ω_{12} were either not observed or are very weak. This is due partially to the greater thickness of the single crystal and consequently more lattice absorption. In the spectrum of one KBr crystal at room temperature a very weak and broad band at about 370 cm^{-1} was found. If this mode is ω_{12}, its amplitude has been severely restricted since KBr is reasonably transparent in this region.

As the amount of space available to the trimer decreases for the series KBr, KCl, and NaCl; an accompanying increase in the frequency of ω_{11} is expected. Although this is true for KBr and KCl, several bands were observed in NaCl which do not fit the simple pattern observed in KCl and which occur at frequencies smaller than ω_{11} in KCl and KBr. Another anomaly exists in KCl and perhaps in KBr. In addition to the components of ω_{11} in KCl two medium intensity bands occur at 752.5 and 744.5 cm^{-1} in samples doped with enriched ^{10}B

and ^{11}B respectively. Although these bands exhibit the same dependence upon boron concentration and thermal history as the trimer and are accompanied by relatively strong "trimer interaction bands," the relative intensity of 752. 5 cm^{-1} is at least three or four times larger than that of 744. 5 cm^{-1}. Nevertheless, 744. 5 cm^{-1} is slightly stronger than 752. 5 cm^{-1} in crystals containing mixtures of boron isotopes. Furthermore, instead of the isotopic components that are expected between these two bands in the latter crystals, there is a band at 732 cm^{-1} of comparable intensity; see the appropriate spectra after quenching in Figure 4. It is interesting that these spectra would be identical with the two superimposed spectra in the enriched ^{10}B and ^{11}B cases, if it were not for the band at 732 cm^{-1} and a greater than anticipated intensity at 752. 5 cm^{-1}. To explain this anomaly, the band at 732 cm^{-1} and the majority of absorption at 752. 5 cm^{-1} have been assigned to the 2^{11}B$+^{10}$B and ^{11}B$+2^{10}$B components of ω_5 which have been made infrared active by the C$_{2v}$ isotopic perturbation. This assignment agrees well with the value of ω_5 for 3^{10}B obtained from the combination $\omega_5 + \omega_9$. Since the band at 744. 5 cm^{-1} and the remainder of the absorbance at 752. 5 cm^{-1} appear to be simultaneously due to the trimer and a species containing one boron atom, they have tentatively been assigned to a motion due to a coupling between a lattice mode and either a translational or librational mode of the trimer which involves only one boron atom.

One of the strongest pieces of evidence for the trimer model is the agreement between the observed components of ω_{11} in KCl and those predicted for a nondegenerate mode. The trimer model predicts that the relative intensities of the four components will be

$$(^{11}P)^3 : 3(^{11}P)^2(^{10}P) : 3(^{11}P)(^{10}P)^2 : (^{10}P)^3 \qquad (5\text{-}2)$$

which, for example, is equivalent to 1:3:3:1 when $^{11}P = 0.5$. The experimental components, in general, fit this pattern yet there are minor discrepancies. These discrepancies are due, at least in part, to overlapping between adjacent components, and between individual components and trimer interaction bands. The latter effect is made evident by the relative increase in intensity of a band at about 770 cm^{-1} and a shift in the high frequency component to the lower frequency of 790.4 cm^{-1} as the intensity of other trimer interaction bands increase. The former effect is greater for the higher frequency components because of a progressive decrease in separation between adjacent components. Quenching which reduces the concentration of trimer ions and therefore interaction between trimer ions, results in less overlapping and closer agreement between the model and experiment. Results of an appropriate quenching experiment are shown in Figure 4 and listed in Table 30. Nevertheless, agreement is still not complete due to residual overlapping and perhaps to a larger than expected intensity in the mixed boron components that

results from an interaction between ω_{11} and the B_1 component of ω_{13} for C_{2v} symmetry. The nonuniform separation between components may also be explained by this interaction as shown schematically in Figure 18.

Table 30. Experimental and theoretical absorbances for ω_{11} of $(BO_2^-)_3$ in KCl with $^{11}P = .547$ at $T \cong 100°$ K.

| $\omega(cm^{-1})$ | Experimental absorbance normalized to one | | Theoretical absorbance |
	Before quench	After quench	
773.6	.132	.128	$(^{11}P)^3$ = .164
781.4	.319	.362	$3(^{11}P)^2(^{10}P)$ = .406
786.9	.371	.378	$3(^{11}P)(^{10}P)^2$ = .336
791.2	.178	.132	$(^{10}P)^3$ = .093

The two out-of-plane E'' fundamentals are infrared inactive under D_{3h} symmetry, but under C_{2v} symmetry the degeneracy is removed and the B_1 component becomes weakly infrared active while A_2 remains inactive. If the C_{3v} site symmetry perturbation is strong enough the inactive out-of-plane modes ($E'' \rightarrow E$ and $A_2 \rightarrow A'$) should become weakly infrared active. The spectra of KCl samples containing isotopically enriched ^{11}B and ^{10}B contain a weak band at 720.5 cm^{-1} and a weak doublet at 720.9 and 724.1 cm^{-1} respectively. The weak bands at 724.1 and 720.9 cm^{-1} are proposed to be the weakly active E ($3^{10}B$) and B_1 ($^{11}B + 2^{10}B$) modes. These two modes apparently overlap in the enriched ^{11}B case as shown in Figure 18. For

samples containing mixtures of boron isotopes the intensity of both

bands, 724.1 cm^{-1} and a band comprising 720.5 and 720.9 cm^{-1}, be-

came more intense relative to the active fundamentals of the $3^{10}B$ and

$3^{11}B$ trimer ions with 720.5 cm^{-1} showing the largest increase. As

the relative number of C_{2v} molecules is increased, the intensity of

the band containing the B_1 components should become larger. The in-

crease in intensity of 724.1 cm^{-1} may be explained by an increase in

the weakly active A' mode of the $^{11}B + 2^{10}B$ trimer. Although the

size of the anticipated increase in the B_1 components is larger than

what is observed, this discrepancy can be explained by the proposed

interaction between ω_{11} and ω_{13}. Values for ω_{13} in KBr and NaCl

were obtained from the Fermi resonance calculations summarized in

Table 26, and they are consistent with the above assignment of ω_{13} in

KCl.

Table 31. ω_{11}^0 and ω_{13}^0 of $(BO_2^-)_3$ in KCl at $T \simeq 100°$ K. (cm^{-1})

	ω_{11}^0	ω_{13}^0
$3^{11}B$	773.5	720.5
$2^{11}B + ^{10}B$	779.4	720.5 A_2
		722.2 B_1
$^{11}B + 2^{10}B$	785.4	722.3 B_1
		724.1 A_2
$3^{10}B$	791.1	724.1

$$\omega_{11} \qquad\qquad \omega_{13}$$

3 "B

791.1 cm^{-1} 724.1 cm^{-1}

2 "B + ^{10}B

1.4
786.6

1.4
A$_2$ 720.9

"B + 2^{10}B

1.7
781.1

1.7
720.5

3^{10}B

773.5 720.5
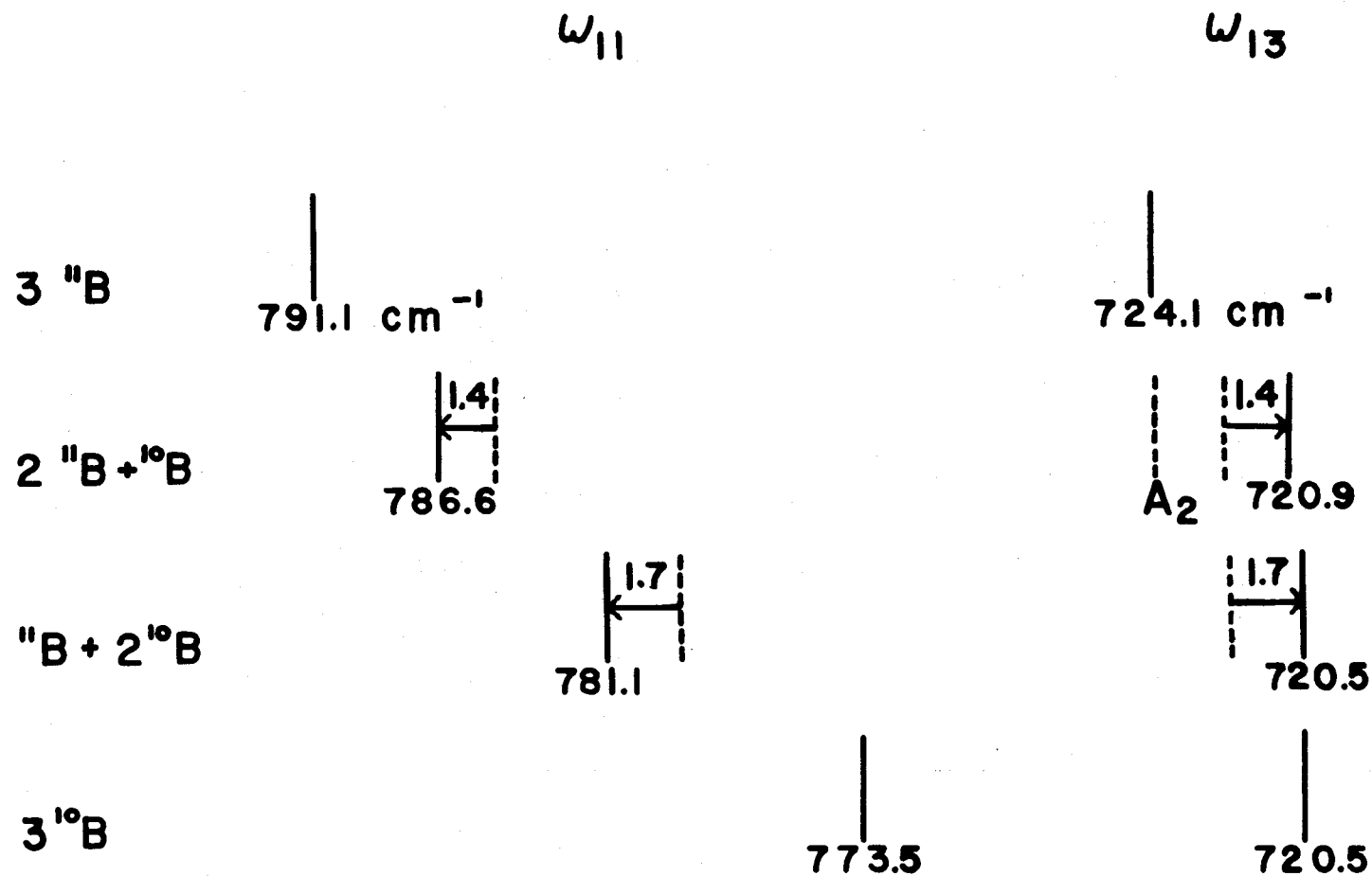
Figure 18.   Interaction between $\omega_{11}(B_1)$ and ω_{13} (A_2+B_1) of $(BO_2^-)_3$ in KCl at $T \simeq 100^\circ$K.   (cm^{-1})

BIBLIOGRAPHY

1.   Adair, T. W. , E. J. Sharp and C. F. Squire.   Magnetic proper-
     ties of lattice imperfections in alkali halide single crystals.
     Journal of Chemical Physics 44:3650-3655.   1966.

2.   Bansigir, K. G. and E. E. Schneider.   Studies on the substruc-
     ture of real crystals by optical and magnetic resonance methods.
     Journal of Applied Physics 33:383-390.   1962.

3.   Beckman Instruments.   IR-7 infrared spectrophotometer in-
     struction manual.   Fullerton, California, 1960.   85 p.

4.   Beckman Instruments.   IR-11 infrared spectrophotometer in-
     struction manual.   Fullerton, California, 1964.   79 p.

5.   Büchler, A. and E. P. Marram.   Gaseous metaborates.   II.
     Infrared spectra of alkali metaborate vapors.   Journal of Chem-
     ical Physics 39:292-295.   1963.

6.   Cole, S. S. , S. R. Scholes and C. R. Ambery.   II.   The system
     R_2O - B_3O_3.   Properties of anhydrous and hydrated metaborates
     of sodium and potassium.   Journal of the American Ceramic
     Society 18:58-61.   1935.

7.   Decius, J. C.   Coupling of the out-of-plane bending mode in ni-
     trates and carbonates of the aragonite structure.   Journal of
     Chemical Physics 23:1290-1294.   1955.

8.   Decius, J. C.   Professor, Oregon State University, Department
     of Chemistry.   Private communication.   Corvallis, 1966.

9.   Decius, J. C.   Relation between force constant and bond length
     for the nitrogen-nitrogen bond.   Journal of Chemical Physics
     45:1069.   1966.

10. Decius, J. C. , O. G. Malan and H. W. Thompson.   The effect of
     intermolecular forces upon the vibrations of molecules in the
     crystalline state.   I.   The out-of-plane bending of the carbonate
     ion in aragonite minerals.   Proceedings of the Royal Society
     275 A:295-309.   1963.

11.   Dingle, T. W. π-electrons in boron-oxygen compounds. In: Progress report no. 12 of the Wave Mechanics and Quantum Theory Group, Mathematical Institute, University of Oxford, Oxford, 1965-1966. Oxford, 1966. p. 73-74.

12.   Dunicz, B. L. Cage structure for polyborate ions. Science 153:737-739. 1966.

13.   Evett, J. and I. Isenberg. DNA-polylysine interaction as studied by polarization of fluorescence. The Annals of the New York Academy of Sciences. (In press)

14.   Fang, Ssu-Mien. The crystal structure of sodium metaborate, $NaBO_2$. Journal of the American Ceramic Society 20:214. 1937.

15.   Fang, Ssu-Mien. The crystal structure of sodium metaborate, $Na_3(B_3O_6)$. Zeitschrift für Kristallographie 99:1-8. 1938.

16.   Fisher, F. , H. Gründig and R. Hilsch. Definierter Einbau und optische Absorption von O_2^- und O^{--} - Zentren in KCl-Kristallen. Zeitschrift für Physik 189:79-96. 1966.

17.   Fisher, H. D. , W. J. Lehmann and I. Shapiro. Trifluoroboroxine: Preparation, infrared spectrum and structure. Journal of Physical Chemistry 65:1166-1168. 1961.

18.   Fredericks. W. J. , F. E. Rosztoczy and J. Hatchett. Investigation of crystal growth processes. Palo Alto, 1963. 24 numb. leaves. (Stanford Research Institute. SRI Project #PAU-3523. Final Report)

19.   Fredericks, W. J. , L. W. Schuerman and L. C. Lewis. An investigation of crystal growth processes. Corvallis, Oregon, 1966. 78 numb. leaves. (Oregon State University. Dept. of Chemistry. Final report on U. S. Air Force Office of Scientific Research Contract AF-AFOSR-217-63 Project 9762-02)

20.   Fritz, B. , F. Lüty and J. Anger. Der Einfluss von OH^- - Ionen auf Absorptionsspektrum und Ionenleitfähigkeit von KCl-Einkristallen. Zeitschrift für Physik 174:240-256. 1963.

21.   Fumi, F. G. and M. P. Tosi. Ionic sizes and Born repulsive parameters in the NaCl-type alkali halides - I. Journal of Physics and Chemistry of Solids 25:31-43. 1964.

22. Gie, T. I. and M. V. Klein. Infrared and ultraviolet OH bands in hydroxide-doped KCl, KBr, NaCl and NaBr. Bulletin of the American Physical Society 8:230. 1963.

23. Goldschmidt, V. M. and H. Hauptmann. Isomorphie von Boraten und Karbonaten. Gottingen Nachrichten, 1932, p. 53-72.

24. Goubeau, J. and D. Hummel. Die Schwingungsspektren verschiedener Borsauerstoffverbindungen. Zeitschrift für Physikalische Chemie, neue Folge, bd. 20:15-33. 1959.

25. Goubeau, J. and H. Keller. Raman-Spektren und Struktur von Boroxol-Verbindungen. Zeitschrift für Anorganische und Allgemeine Chemie 272:303-312. 1953.

26. Hatcher, J. T. and L. V. Wilcox. Colorimetric determination of boron using carmine. Analytical Chemistry 22:567-569. 1950.

27. Herzberg, Gerhard. Molecular spectra and molecular structure. II. Infrared and Raman spectra of polyatomic molecules. Princeton, New Jersey, D. Van Nostrand, 1966. 632 p.

28. Hisatsune, I. C. and N. H. Suarez. Infrared spectra of metaborate monomer and trimer ions. Inorganic Chemistry 3:168-174. 1964.

29. Latimer, B. and J. P. Devlin. Vibrational spectra for fluorine and chlorine derivatives of boroxine. Spectrochimica Acta 21:1437-1444. 1965.

30. Mazerio, M., H. A. Plettinger and W. H. Zachariasen. The bond lengths in the sodium metaborate structure. Acta Crystallographia 16:594-595. 1963.

31. McDonald, R. S. Line absorption in the IR spectrum of NaCl. Spectrochimica Acta 15:773. 1959.

32. Morgan, H. W. and P. A. Staats. Infrared spectra of dilute solid solutions. Journal of Applied Physics 33:364-366. 1962.

33. Parsons, J. L. Vibrational spectra of orthorhombic metaboric acid. The Journal of Chemical Physics 33:1860-1866. 1960.

34. Pauling, Linus. The nature of the chemical bond. 3d ed. Ithaca, New York, Cornell University Press, 1960. 644 p.

35. Perkin-Elmer Corporation. Model 450 instructional manual. Norwalk, Connecticut, 1965. 145 p.

36. Plint, C. A. and L. W. Watson. Temperature dependence of light scattering in KCl:Pb. Bulletin of the American Physical Society 11:811. 1966.

37. Rolfe, J. Infrared and ultraviolet absorption bands in KBr crystals containing hydroxide ion impurity. Canadian Journal of Physics 41:1525-1527. 1963.

38. Squire, C. F. and E. R. Zamechi. Optical birefringence in alkali halides. Journal of Chemical Physics 47:4888-4890. 1967.

39. Steele, W. C. and J. C. Decius. Infrared absorption of lanthanum, scandium and indium borate and the force constants of borate ion. Journal of Chemical Physics 25:1184-1188. 1956.

40. Taurel, L. and Girard-Nottin. Rôle des dislocations dans la diffusion de la lumière par les halogénures alcalins. Journal de Physique, sup. C-3, Vol. 27:25-29. 1966.

41. Weir, C. E. and R. A. Schroeder. Infrared spectra of the crystalline inorganic borates. Journal of Research of the U. S. National Bureau of Standards, Sec. A, Physics and Chemistry 68A:465-487. 1964.

42. Wells, A. F. Structural inorganic chemistry. 3d ed. London, Oxford University, 1962. 590 p.

43. Wilson, E. Bright, J. C. Decius and Paul C. Cross. Molecular vibrations. New York, McGraw-Hill, 1955. 388 p.

44. Zachariasen, W. H. The crystal lattice of calcium metaborate, CaB_2O_4. Proceedings of the National Academy of Sciences 17: 617-619. 1931.

45. Zachariasen, W. H. The crystal structure of potassium metaborate, $K_3(B_3O_6)$. Journal of Chemical Physics 5:919-922. 1937.

46. Zachariasen, W. H.   Refinement of the calcium metaborate structure.   Acta Crystallographica 16:390-392.   1963.

47. Zachariasen, W. H. and G. E. Zieger.   The crystal structure of calcium metaborate, CaB_2O_4.   Zeitschrift für Kristallographie 83:354-362.   1932.

APPENDICES

APPENDIX I

Internal Symmetry Coordinates of the Metaborate Trimer for D_{3h} Symmetry

In-Plane

Symmetry Species

A_1'

$$S_1 = 1/\sqrt{3}(r_1 + r_2 + r_3)$$

$$S_2 = 1/\sqrt{3}(K_1^{A_1} + K_2^{A_1} + K_3^{A_1})$$

$$S_3 = 1/\sqrt{3}(\beta_1 + \beta_2 + \beta_3)$$

A_2'

$$S_4 = 1/\sqrt{3}(K_1^{B_2} + K_2^{B_2} + K_3^{B_2})$$

$$S_5 = 1/\sqrt{3}(a_1^{B_2} + a_2^{B_2} + a_3^{B_2})$$

E'

$$S_6 = 1/\sqrt{6}(2r_1 - r_2 - r_3)$$

$$S_7 = 1/\sqrt{6}(2K_1^{A_1} - K_2^{A_1} - K_3^{A_1})$$

$$S_8 = 1/\sqrt{2}(K_2^{B_2} - K_3^{B_2})$$

$$S_9 = 1/\sqrt{6}(2\beta_1 - \beta_2 - \beta_3)$$

$$S_{10} = 1/\sqrt{2}(a_2^{B_2} - a_3^{B_2})$$

E' $S_{11} = 1/\sqrt{2}(r_2 - r_3)$

$$S_{12} = 1/\sqrt{2}(K_2^{A_1} - K_3^{A_1})$$

$$S_{13} = 1/\sqrt{6}(2K_1^{B_2} - K_2^{B_2} - K_3^{B_2})$$

$$S_{14} = 1/\sqrt{2}(\beta_2 - \beta_3)$$

$$S_{15} = 1/\sqrt{6}(2a_1^{B_2} - a_2^{B_2} - a_3^{B_2})$$

Out-of-Plane

Symmetry Species

A_2'' $S_{16} = 1/\sqrt{3}(z_1 + z_2 + z_3)$

$$S_{17} = 1/\sqrt{3}(Z_1 + Z_2 + Z_3)$$

E'' $S_{18} = 1/\sqrt{6}(2z_1 - z_2 - z_3)$

$$S_{19} = 1/\sqrt{6}(2Z_1 - Z_2 - Z_3)$$

E'' $S_{20} = 1/\sqrt{2}(z_2 - z_3)$

$$S_{21} = 1/\sqrt{2}(Z_2 - Z_3)$$

where

$$K_1^{A_1} = 1/\sqrt{2}(s_1 + s_2) \qquad K_1^{B_2} = 1/\sqrt{2}(s_1 - s_2)$$

$$K_2^{A_1} = 1/\sqrt{2}(s_3 + s_4) \qquad K_2^{B_2} = 1/\sqrt{2}(s_3 - s_4)$$

$$K_3^{A_1} = 1/\sqrt{2}(s_5 + s_6) \qquad K_3^{B_2} = 1/\sqrt{2}(s_5 - s_6)$$

$$a_1^{A_1} = 1/\sqrt{2}(a_1 + a_2) \qquad a_1^{B_2} = 1/\sqrt{2}(a_1 - a_2)$$

$$a_2^{A_1} = 1/\sqrt{2}(a_3 + a_4) \qquad a_2^{B_2} = 1/\sqrt{2}(a_3 - a_4)$$

$$a_3^{A_1} = 1/\sqrt{2}(a_5 + a_6) \qquad a_3^{B_2} = 1/\sqrt{2}(a_5 - a_6)$$

Internal Symmetry Coordinates of the Metaborate Trimer for C_{2v} Symmetry

In-Plane

Symmetry Species

A_1

$$S_1 = r_1$$

$$S_2 = 1/\sqrt{2}(r_2 + r_3)$$

$$S_3 = K_1^{A_1}$$

$$S_4 = 1/\sqrt{2}(K_2^{A_1} + K_3^{A_1})$$

$$S_5 = 1/\sqrt{2}(K_2^{B_2} - K_3^{B_2})$$

$$S_6 = \beta_1$$

$$S_7 = 1/\sqrt{2}(\beta_2 + \beta_3)$$

$$S_8 = 1/\sqrt{2}(a_2^{B_2} - a_3^{B_2})$$

$$B_2 \qquad S_9 = 1/\sqrt{2}(r_2 - r_3)$$

$$S_{10} = 1/\sqrt{2}(K_2^{A_1} - K_3^{A_1})$$

$$S_{11} = K_1^{B_2}$$

$$S_{12} = 1/\sqrt{2}(K_2^{B_2} + K_3^{B_2})$$

$$S_{13} = 1/\sqrt{2}(\beta_2 - \beta_3)$$

$$S_{14} = \alpha_1^{B_2}$$

$$S_{15} = 1/\sqrt{2}(\alpha_2^{B_2} + \alpha_3^{B_2})$$

Out-of-Plane

Symmetry Species

$$A_2 \qquad S_{16} = 1/\sqrt{2}(z_2 + z_3)$$

$$S_{17} = 1/\sqrt{2}(Z_2 + Z_3)$$

$$B_1 \qquad S_{18} = z_1$$

$$S_{19} = 1/\sqrt{2}(z_2 + z_3)$$

$$S_{20} = Z_1$$

$$S_{21} = 1/\sqrt{2}(Z_2 + Z_3)$$

F Matrix for the D_{3h} Internal Symmetry Coordinates of the Metaborate Trimer

F	S_1	S_2	S_3	S_4	S_5	S_6	S_7	S_8	S_9	S_{10}
S_1	ϕ_r	$\sqrt{2}\phi_s'$	$s\phi_{r\beta}$							
S_2	$\sqrt{2}\phi_s'$	$\phi_s+\phi_s'$	$\sqrt{2}s\phi_{r\beta}'$							
S_3	$s\phi_{r\beta}$	$\sqrt{2}s\phi_{r\beta}'$	$s^2\phi_\beta$							
S_4				$\phi_s-\phi_s'$	$(rs)^{\frac{1}{2}}(\phi_{r\beta}'-\phi_{r\beta})$					
S_5				$(rs)^{\frac{1}{2}}(\phi_{r\beta}'-\phi_{r\beta})$	$rs(\phi_\beta-\phi_\beta')$					
S_6						ϕ_r	$\sqrt{2}\phi_s'$	0	$s\phi_{r\beta}$	0
S_7						$\sqrt{2}\phi_s'$	$\phi_s+\phi_s'$	0	$\sqrt{2}s\phi_{r\beta}'$	0
S_8						0	0	$\phi_s-\phi_s'$	0	$(rs)^{\frac{1}{2}}(\phi_{r\beta}'-\phi_{r\beta})$
S_9						$s\phi_{r\beta}$	$\sqrt{2}s\phi_{r\beta}'$	0	$s^2\phi_\beta$	0
S_{10}						0	0	$(rs)^{\frac{1}{2}}(\phi_{r\beta}'-\phi_{r\beta})$	0	$rs(\phi_\beta-\phi_\beta')$

F	S_{16}	S_{17}	S_{18}	S_{19}
S_{16}	$s^2(\phi_z + 2\phi_z')$	$s^2(\phi_{zZ} + 2\phi_{zZ}')$		
S_{17}	$s^2(\phi_{zZ} + 2\phi_{zZ}')$	$s^2(\phi_Z + 2\phi_Z')$		
S_{18}			$s^2(\phi_z - \phi_z')$	$s^2(\phi_{zZ} - \phi_{zZ}')$
S_{19}			$s^2(\phi_{zZ} - \phi_{zZ}')$	$s^2(\phi_Z - \phi_Z')$

APPENDIX III

Calculated Eigenvalues (cm^{-1}) of Metaborate Trimer with $\underline{D}_{3h}$ Symmetry Using Various Values for the Force Constants; $\underline{\phi}_\beta, \underline{\phi}_{r\beta}$ and $\underline{\phi}_{r\beta}'$

	$\phi_{r\beta} = .25$				$\phi_{r\beta}' = 1.00$			
	^{11}B				^{10}B			
ϕ_β	.40	.60	.80	1.00	.40	.60	.80	1.00
A_1'	1318	1338	1361	1387	1357	1379	1404	1432
	903	926	950	972	903	927	951	974
	174	295	367	417	177	300	372	423
A_2'	1224	1224	1224	1224	1255	1255	1255	1255
	756	756	756	756	768	768	768	768
E'	1318	1340	1363	1388	1358	1382	1407	1434
	1111	1114	1117	1120	1151	1154	1156	1158
	985	987	988	990	989	990	992	994
	402	403	403	409	403	403	404	410
	155	269	340	389	158	272	344	393

	$\phi_{r\beta} = -.25$				$\phi_{r\beta}' = .50$			
	^{11}B				^{10}B			
ϕ_β	.40	.60	.80	1.00	.40	.60	.80	1.00
A_1'	1292	1308	1327	1349	1333	1351	1372	1396
	798	826	858	891	799	827	858	891
	358	441	495	532	364	448	502	539
A_2'	1224	1224	1224	1224	1255	1255	1255	1255
	756	756	756	756	768	768	768	768
E'	1304	1330	1357	1385	1345	1373	1402	1432
	1135	1137	1139	1140	1170	1170	1171	1172
	1009	1009	1009	1009	1019	1020	1020	1020
	404	406	413	441	405	407	417	446
	267	336	381	396	270	339	383	397

	$\phi_{r\beta} = -.50$				$\phi_{r\beta}' = .25$			
	^{11}B				^{10}B			
ϕ_β	.40	.60	.80	1.00	.40	.60	.80	1.00
A_1'	1284	1298	1315	1335	1324	1341	1360	1382
	741	767	801	840	741	767	801	840
	408	494	548	581	415	501	555	588
A_2'	1224	1224	1224	1224	1255	1255	1255	1255
	756	756	756	756	768	768	768	768
E'	1311	1338	1367	1396	1351	1381	1411	1443
	1146	1146	1147	1147	1176	1176	1177	1177
	1012	1012	1012	1012	1025	1025	1025	1025
	409	414	427	451	411	416	430	456
	272	333	372	388	275	336	373	388

APPENDIX IV

L^{-1} Matrices for the Metaborate Trimer with D_{3h} Symmetry

These transformations are for the trimer of metaborate when all three boron atoms are ^{11}B or ^{10}B with the following assumed values for the force constants:

$$\phi_\beta = .80 \text{ md/Å}$$

$$\phi_{r\beta} = -.50 \text{ md/Å}$$

$$\phi_{r\beta}' = .25 \text{ md/Å}$$

The first set of out-of-plane force constants in Table 22.

The normal coordinates Q and internal symmetry coordinates S which are related by means of the linear transformation L^{-1} according to Equation (4-6) are the column matrices

$$Q^\dagger = (Q_1 Q_2 Q_3 Q_4 Q_5 Q_6 Q_7 Q_8 Q_9 Q_{10} Q_{11} Q_{12} Q_{13} Q_{14}) \qquad (6\text{-}1)$$

and

$$S^\dagger = (S_1 S_2 S_3 S_4 S_5 S_6 S_7 S_8 S_9 S_{10} S_{16} S_{17} S_{18} S_{19}) \qquad (6\text{-}2)$$

in which Q_i and S_i are the observed normal modes and the internal symmetry coordinates for D_{3h} symmetry described in Appendix I.

^{10}B

L^{-1}

2.07	-.70	.06
.89	3.38	1.35
3.30	3.06	-2.14

| 2.10 | .08 |
| 1.22 | 2.01 |

1.51	-1.19	.37	.14	.06
1.33	.77	-1.67	-.15	.25
1.91	2.26	.32	-.03	-.70
2.18	.84	3.80	-2.28	2.43
-.68	3.77	2.51	3.34	2.24

| -1.02 | .83 |
| 4.06 | -1.30 |

| 2.41 | 1.75 |
| -1.25 | .13 |

^{11}B

L^{-1}

2. 17   -. 69   . 05

 . 88   3. 38   1. 35

3. 24   3. 15   - 2. 17

                    2. 18   . 14

                    1. 10   2. 04

                              1. 53   -1. 27   . 42   . 13   . 07

                              1. 62   1. 02   -1. 64   -. 17   . 17

                              1. 74   2. 14   . 59   . 001   -. 74

                              2. 12   . 99   3. 93   -2. 21   2. 50

                              -. 74   3. 73   2. 34   3. 43   2. 16

                                                  -1. 09   . 86

                                                  4. 07   -1. 29

                                                            2. 41   1. 75

                                                            -1. 34   . 11